SUMMARY OF PROFESSIONAL ACCOMPLISHMENTS

Dr Sławomir Jabłoński

Institute of Plasma Physics and Laser Microfusion
Hery 23, 01-497 Warsaw, Poland

SUMMARY OF PROFESSIONAL ACCOMPLISHMENTS

Personal data:

Name and surname: **Sławomir Jabłoński**

Date and place of birth: 15.03.1961 Milanówek

Place of employment: S.Kaliski Institute of Plasma Physics and Laser Microfusion, Hery Street 23, 01-497 Warsaw, Poland

Diplomas, scientific degrees:

Master of Science in chemistry, 1986

University of Warsaw, Faculty of Chemistry

Title of the dissertation:

„Using of the isopropyl cyclohexyl carbodiimide in peptide synthesis"

Doctor of Philosophy in physics, 1998

Warsaw University of Technology, Faculty of Physics and Mathematics

Title of the dissertation:

„Generation of short pulses of light in excimer lasers"

Dissertation supervisor: Prof. dr hab. Jan Badziak

Reviewers: Prof. dr hab. Adam Kujawski

                                       Dr hab. Jan Owsik

Information on employment in research units

since 2017	Senior researcher in Department of Nuclear Fusion and Plasma Spectroscopy of Institute of Plasma Physics and Laser Microfusion
1998 – 2017	Senior researcher in Department of Laser Fusion of Institute of Plasma Physics and Laser Microfusion
1991 – 1998	Assistant in Department of Laser Plasma of Institute of Plasma Physics and Laser Microfusion
1986 – 1991	Assistant in Independent Laboratory of Technology of Institute of Plasma Physics and Laser Microfusion

The achievement justifying the application for habilitation, as defined in Art. 16, Par. 2 of the Act of 14 March 2003 on Academic Degrees and Academic Title and on Degrees and Title in Arts

a.) title of the scientific achievement

"Investigation of plasma acceleration processes using high power lasers ($I_L < 10^{19}$W/cm^2) and extra high-power lasers ($I_L \geq 10^{19}$W/cm^2) by the use of computer modeling"

b.) introduction to the summary:

Energetic ion beams generated at the interaction of high-intensity lasers with solid targets have the potential to be applied in various areas of science, technology, and medicine. These possible ion beam applications can be roughly divided in two groups. The first one - which includes, for example, nuclear and particle physics, hadron therapy of cancers, and proton radiography - requires high ion energies (from tens to hundreds of mega-electron-volts and beyond) and, possibly, a narrow ion energy spectrum, while ion beam powers P_i and intensities I_i can be moderate. In the second group - which includes high energy-density physics (HEDP) and fast ignition (FI) of inertial fusion, as well as ion implantation or radioisotope production for positron emission tomography - mean ion energies <10 MeV are sufficient but ion beam powers and intensities should be very high. For instance, FI requires a proton beam of the mean proton energy $<E_i> \sim 3–5$ MeV, $I_i > 5$ x 10^{19} W/cm^2, and $P_i \sim 1$ PW. Although in the last group of applications monoenergetic ion beams are usually not necessary, some control of the ion energy spectrum is needed as well. For both groups of applications, collimated or focused beams are commonly demanded.

A recognized laser method of production of collimated, high-ion-energy beams is target normal sheath acceleration (TNSA). In this method, ions are accelerated at the rear surface of the foil target by a virtual cathode (Debye sheath) created by hot electrons produced by a laser at the target front and penetrating through the target. It has been demonstrated by several research groups that at relativistic laser intensities I_L (i.e., at $I_L\lambda^2_L > 10^{18}$ W cm^{-2} μm^2, where λ_L is the laser wavelength) TNSA can produce collimated ion beams of maximum energies of tens of mega-electron-volts for protons or of several mega-electron-volts per atomic mass unit for heavier ions. Generation of quasimonoenergetic ($\Delta E_i/<E_i> \sim 10\%$) ion (proton) beams has been demonstrated as well. However, the ion density of TNSA beams is relatively low ($< 10^{19}$ cm^{-3}) and, as a result, the ion beam intensity $I_i = n_i \cdot v_i \cdot E_i$, or current density $j_i = Z \cdot e \cdot n_i \cdot v_i$ is usually moderate ($Z -$ is ion charge state, e is the elementary charge, n_i, v_i, and E_i are ion density, velocity, and energy, respectively).

For producing high-intensity high-power ion beams for the second group of application, skin-layer ponderomotive acceleration (SLPA) (also referred to as radiation pressure acceleration) seems to be a more promising method. In this method, ponderomotive forces induced by a short laser pulse near the critical plasma surface drive dense plasma bunches (blocks) of ion densities comparable to (or higher than) the plasma critical density. As these densities are about a thousand times higher than those produced by TNSA, even at moderate ion energies the intensities and current densities of SLPA-driven ion beams can be extremely high, much higher than in the case of TNSA beams produced at comparable laser intensities and/or energies. Very high intensity of the SLPA beam coupled to a very short (picosecond/subpicosecond) duration of the ion pulse at the source creates a viable prospect for application of ion beams driven by SLPA in HEDP and for FI of fusion targets.

The reported scientific achievement concerns research into various aspects of the use of SLPA as an efficient source of ion beams with high intensity and current density. In my work I undertook research on such issues as optimization of acceleration in terms of efficiency of energy transfer from laser beams to driven ionic targets, examination of innovative conditions for acceleration process (study of the new Light Induced Cavity Pressure Acceleration (LICPA) method, developed by our group), examining the effects associated with acceleration, eg rippling effect, ion dispersion effect, etc. All investigations were based on own numerical codes improved over the years of work. As part of the work, I created both hydrodynamic codes 1D and 2D (for medium and low intensity lasers ($<10^{19}$ W/cm^2) and large ($>>10^{19}$ W/cm^2) lasers.

The results of my numerical work completed by experiments conducted by my colleagues and other scientific groups in the world confirmed the expectations of the SLPA method. More detailed descriptions of specific cases can be found in the description of the "Outline of a scientific career" on pages 8 - 31. The list of references can be found in the chapter "References" on pages 36 - 39 (items: [A01] - [A24]).

Outline of a scientific career

In 1986 I began working as an assistant in the Independent Laboratory of Technology of the Institute of Plasma Physics and Laser Microfusion in Warsaw.

In the years 1986-1988 I dealt with the following issues:
- development of a technology for the manufacture of plastic targets for laser-target experiments devoted to investigation of production and compression of plasma (cannonball targets and flat targets of requested thicknesses)
- creation of the computer code for modeling of a thin dielectric layer stacks dedicated to elimination of the reflections from optical elements. The results provided by the code were used for manufacturing of such stacks with the use of sputtering method.

The first topic included the efficient production of a spherical microcapsules of a diameter of 500 μm to 1000 μm made of polyethylene (PE) or polystyrene (PS), in which there were drilled holes and spherical glass microcapsules put in the center (diameter about 250 μm).

During the experiment, the central glass target was exposed to a multi-beam laser light, through the holes in the, plastic shell which was responsible for recycling the dissipating plasma and energy, leading to an increase in the coefficient of the energy transfer from the laser to the central target.

In the case of flat targets, the main task was to refine the methodology for the production of thin (micrometer) plastic discs of uniform and controlled thickness. The results of the work were presented in the internal reports available at the Institute of Plasma Physics and Laser Microfusion.

The second project was related to the processing technologies of optical elements used in laser systems. As is commonly known, there are two types of problems. First of all, how to produce transmission optics in which the reflection of electromagnetic radiation (EM) from the surface should be as small as possible (lenses, prisms, etc.) and second of all, how to produce effective reflection systems (mirrors). In both of those issues, the effective solution is to produce dielectric layers of appropriate parameters (strictly defined thickness and refractive index)on the surface of optical elements. Effective formation of such layers requires detailed modeling of the physics of such thin-layer stacks. For that purpose I created a special code that made such predictions possible. As part of the code, I incorporated full complex refractive indexes that also included light absorption in the material of each layer. The quality of the generated code has been fully confirmed by experiments in which transmission measurements of thin-layer stacks (up to a dozen or so layers) were made. The results from the model proved to be perfectly compatible with the experiment. The code was used for many years, according to my knowledge, at the Institute of Plasma Physics and Laser Microfusion and later at the Institute of Quantum Electronics in the thin-layer sputtering laboratory.

In the years 1988-1991 I dealt with the following issues:
- diffusion technology of integrated optoelectronic components based on titanium diffusion into a matrix made of lithium niobate
- computer modeling of integrated optoelectronics (waveguide couplers, Y-type splitters and optical modulators)

As part of the technological theme, I was involved in the production of planar waveguides in a matrix made of lithium niobate $LiNbO_3$. The scope of work included the design of special masks for selective application of titanium Ti layers to the designated spots on the niobate matrix, and subsequent diffusion of such layers during the high temperature diffusion process.

The widths of typical tracks were about 1 μm, and the entire optoelectronic elements measured 2 x 3 cm.

The technological process was preceded by a computer modeling. For this purpose, I created a special 2D code to track the propagation of electromagnetic waves in dielectric materials with a given indicatrix of the refractive index and the required profile of the diffused Ti. The code made it possible to obtain the optimum planar waveguide widths for a given length of light and for a single-mode propagation. Optimal angles of the Y-type splitters, at which the light propagation has the smallest losses at the branching point, were also calculated with the use of this code. In addition, I analyzed the optimum distances between single-mode planar waveguides for reaching the most efficient light beam penetration between the said waveguides for the assumed coupling distance (integrated planar coupler analysis). The results of this research were published in IPPLM internal reports.

In the years 1991-1998 I dealt with the following issues:
- computer modeling of short pulse generation in excimer lasers

During the last decade of the 20th century, the topic of effective generation of short pulsed laser (ps or shorter) aroused and is still arousing considerable interest worldwide. The most successful and popular method of generating such pulses in those years was mode locking. The characteristic common feature of almost all versions of this method applied hitherto is that variations in the temporal and spectral distributions of the light intensity during one cavity round-trip were rather slight. Thus, forming a well-defined short pulse or, in other words, locking of a large number longitudinal modes of the laser required numerous (usually a few hundred or more) round-trips of light in the cavity. Therefore, the short pulse formation process was relatively slow and required microseconds or more. Such kind of mode locking can be called Slow Mode Locking (SML) and can be applied successfully in long-pulse-pumped storage lasers, such as Nd:glass, or, even more effectively, cw lasers. In the case where the gain duration in the active medium is short (excimer lasers, CO_2 laser), it was necessary to create conditions in which changes in the temporal and spectral distributions of the light intensity during one cavity round-trip, resulting from periodic modulation of the cavity losses, are great. This is feasible particularly when the duration, τ_m, of the transmission window produced by a modulator is much shorter than the cavity round-trip time, T_c. In this case, the modulator enforces in the cavity the appearance of the intensity temporal distribution of duration $\tau \sim \tau_m$, much shorter than T_c. The spectrum of a pulse formed in such a way is determined by its Fourier transform and can include many cavity modes ($\Delta\nu \gg 1/T_c$). Such mode locking can be called Fast Mode Locking (FML).

In principle, FML can be accomplished with the use of Pockels cells (PC) driven by square-wave voltage. However, due to the limitations on the switching time, ts, of the voltage on the PC ($\tau_m \sim \tau_s > 10^{-10}$s) and a relatively low contrast ratio of PC-modulators ($\sim 10^2$), more complex active-passive mode locking is necessary in this case to obtain pulses shorter than 10^{-11}s in short-gain-duration lasers. The above mentioned limitations appear to a much slighter degree when implementing electro-optic deflectors (EODs). Hence, one could expect that the application of FML with an EOD in short-gain-duration wide-bandwidth lasers, such as excimer lasers, would make it possible to obtain pulses of duration in the pico- or subpicosecond range. Fig.1 illustrates the principle of for the method described above.
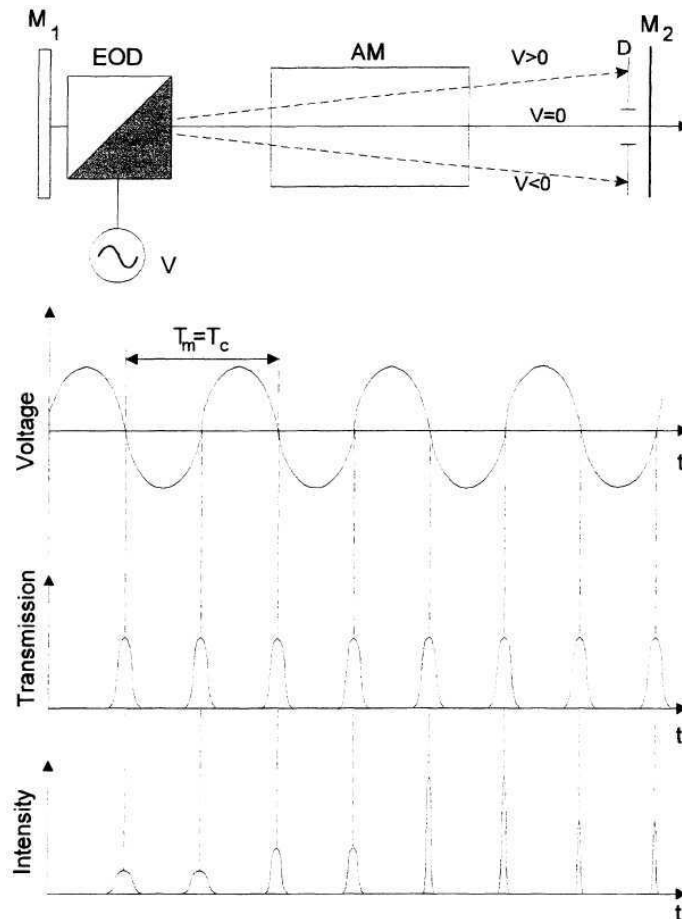
Fig.1 Schematic diagram and the principle of operation of a short-pulse laser with fast mode locking using an electro-optic deflector. AM – active medium; EOD – electro-optic-deflector; D – diaphragm; M_1, M_2 – mirrors; V – voltage; T_c – cavity round-trip time; modulation period T_m.

In the time period mentioned above, I worked on computer modeling of such processes. I have created a comprehensive concept of pulse generation using the XeCl and KrF lasers that work with electro-optical deflectors. In the computer code I wrote, the characteristics of the energy levels of the active laser mediums, were taken into account. Among others, the model included, among others, lifetimes of energy levels, cross-section values for stimulated and spontaneous emission. Additionally, models of a passive (saturable dye absorbers) and active light modulators (electro-optic deflectors), responsible for mode-locking effect, were added. Various parameter types of the mentioned systems were analyzed in the context of the efficiency of the short pulses generation. Exemplary results obtained during the analysis of the deflection angle of EOD for short pulse generation are presented in Fig.2.
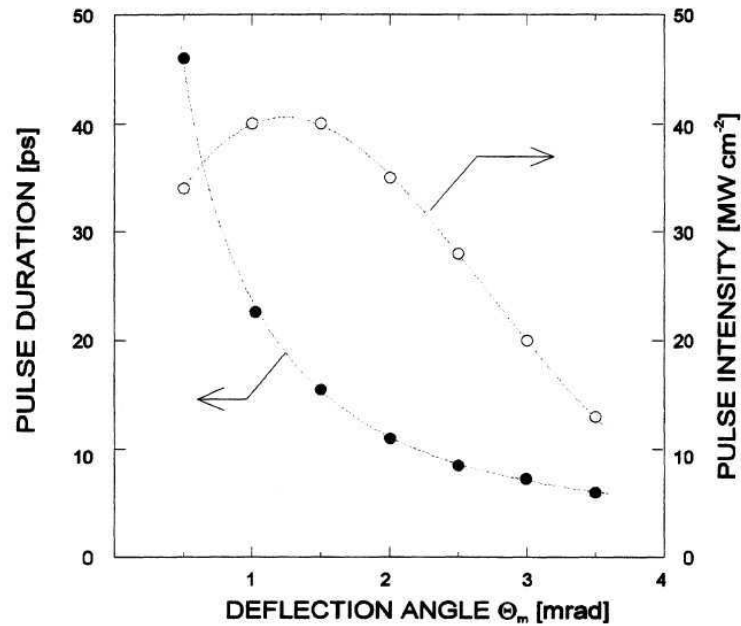
Fig.2 The dependence of the peak intensity and duration of a pulse generated from the XeCl
laser on the maximum deflection angle. $T_m=T_c$, $T_{pump}= 50$ ns, $R_2= 0.2$, $g_0L= 4$
(g_0L small-signal-gain-length product at the maximum of pumping pulse).

As a result of the study, we have developed a comprehensive method of producing ultraviolet pulses (248 nm KrF, 308 nm XeCl) with duration of pico and subpicoseconds. At that time, it was a very significant achievement. The results of the work carried out during this time were collected and presented in my dissertation „*Modeling of short pulse generations in excimer lasers*" and published in several scientific journals [B-01 – B-06]. The idea itself of generation of a short pulses has been patented [PL 181759 B1].

In the years 1999-2015 I dealt with the following issues (description of scientific achievements within the meaning of Article 16 paragraph 2 of the Act):

- computer modeling of plasma acceleration processes using high power lasers ($I_L < 10^{19}$W/cm^2) based on my own hydrodynamic codes (1D and 2D) in a non-relativistic and relativistic approach,
- computer modeling of plasma acceleration processes using extra high-power lasers ($I_L \geq 10^{19}$W/cm^2) based on my own 1D and 2D particle-in-cell codes (PIC), in a relativistic approach.

In the years 1999-2003, I was involved in the creation of a two-dimensional, two-fluid non-relativistic 1D hydrodynamic code that simulates the interaction of a laser beams with solid state targets. The model included, among others, the impact of ion and electron collisions. The model made it possible to analyze different preplasma profiles (linear or exponential) as well as various laser beam parameters (envelope shapes of beams and pulses as well as their intensities and durations).

The described code was used in the works on the generation of ion beam bundles with ultra-high current density values obtained by the interaction of short laser pulses ($\tau_L < 1$ps) of intensity of $\sim 10^{17}$-10^{18}W/cm^2 and energies ≤ 1J [A-01, A-02].

The idea of producing ultrahigh-current-density ion beams by the skin-layer interaction is illustrated in Fig. 3. On the target surface the laser prepulse produces a preplasma layer of the thickness L_{pre} at least several times smaller than the laser focal spot diameter d_f. The main laser pulse interacts most intensively with the plasma in the skin layer near the surface of the critical electron density $n_{ec} = m_e \omega^2 / 4\pi e^2$ (ω is the laser frequency) and the geometry of the interaction is almost planar ($L_{pre} \ll d_f$). The high plasma density gradient in the interaction region produces nonlinear ponderomotive forces acting at the laser beam incidence perpendicularly to the target surface, and so nearly parallel to the normal vector to the surface. The force density f_{NL} can be more or less expressed as one-dimensional negative gradient of the electromagnetic energy density of the laser field given by its (dielectric modified) electric and magnetic vectors $\mathbf{E}$ and $\mathbf{H}$: $f_{NL} = -(\partial/\partial x)(\mathbf{E}^2 + \mathbf{H}^2)/8\pi$. The gradients of the energy density near the critical surface result in two opposite nonlinear forces which break the plasma and drive two thin ($\sim \lambda$) plasma blocks toward the vacuum and toward the plasma interior, respectively (λ is the laser wavelength). The density of the plasma blocks is high (the ion density $n_i \approx n_{ec} / z$, where z is the ion charge state) but the electron temperature is fairly moderate at subrelativistic laser intensities.
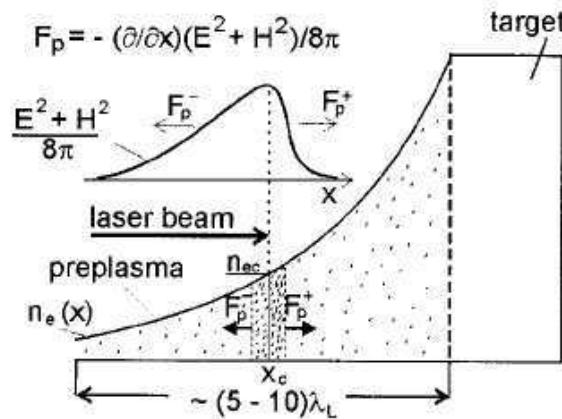

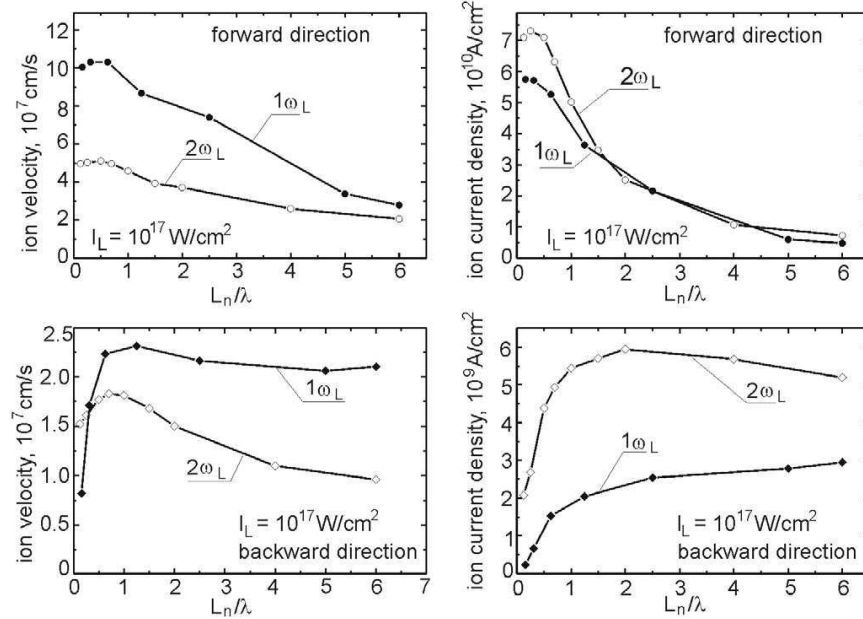Fig.3 The priciple of ultrahigh-current-density ion beams production.

Fig.4 The velocities and the densities of ion currents driven by a 1 ps laser pulse as a function of the plasma density gradient scale length.

As it has been shown both numerically and experimentally, it is possible to obtain extremely high ion currents of $\geq 10^{10}$ A/cm^2. Moreover, the dominant effect of this type of acceleration is the ponderomotive force acting in the plasma critical density area (S-LPF). Additionally, it has been shown that the attainable density of ion currents is comparable and even higher than that of a short-pulse beam relativistic beam and acceleration based on TNSA (target normal sheath acceleration).

During the next stage of the research, different scenarios of interaction of laser beams with hydrogen shields were analyzed using simulation [A-03]. As a result of the calculations, the ion velocities and ion current densities were determined as a function of the laser beam intensity ($I_L \sim 10^{16}$ - 10^{17} W/cm^2), both for the beam EM direction and for the opposite direction. The dependence of the above-mentioned parameters on the laser pulse length for ranges from sub-picoseconds to 2 ps was also determined. Fig.5 and Fig.6 present exemplary results of the research [A-03].
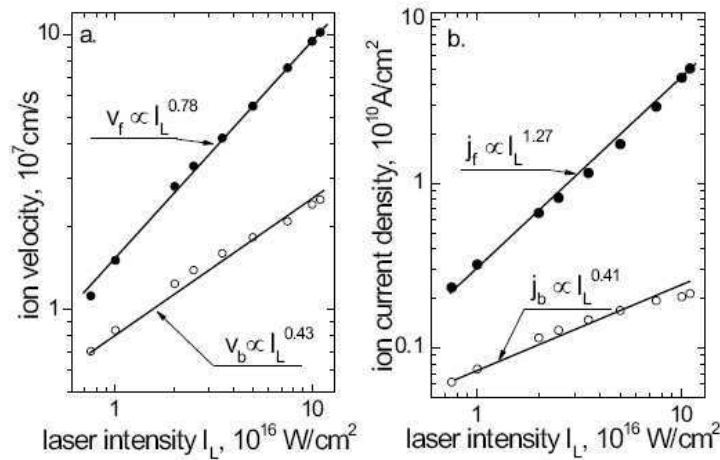
Fig.5 The maximum ion velocities (a) and the maximum ion current densities (b) for backward-emitted (v_b, j_b) and forward-emitted (v_f, j_f) ions as a function of the laser intensity τ_L=1 ps, $L_n/\lambda = 1$.
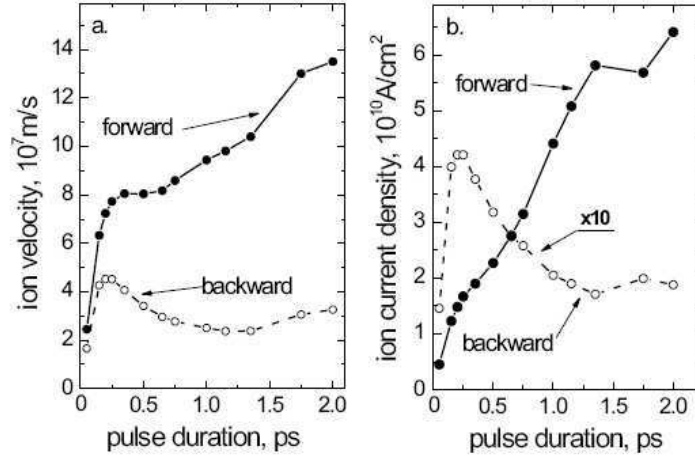
Fig.6   The maximum ion velocities (a) and the maximum ion current densities (b) as a function of the laser pulse duration $L_n/\lambda = 1$.

The further development of the work aimed at analyzing the emission of dense hydrogen ion beams from large Z targets (Au targets), polystyrene targets (PS) and combined (PS / Au) targets. Both backward and forward acceleration based on S-LPF mechanism for laser beams of intensity up to $2*10^{17}$W/cm^2 and duration of $\tau_L=1$ ps were evaluated [A-04]. The work was experimental and numerical. Calculations were made using the 1D code and the new 2D hydrodynamic code based on the advanced two-fluid model by Hora, Aydin and Boreham. In the course of the work, it was confirmed that an efficient generation of well collimated high density ionic beams, using the S-LPA mechanism, is possible, which opens the way for experiments in high energy density physics, inertial fusion, and X-ray laser experiments, without the need of a powerful research infrastructure. Fig.7 presents 2D spatial distribution of the ion current density near the critical surface produced by a 200-fs laser pulse of intensity 10^{16} W/cm^2.
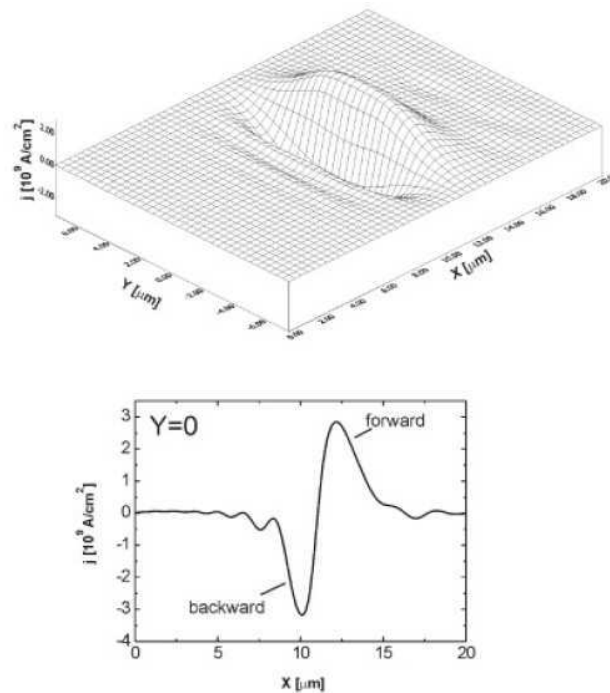

Fig.7 Two-dimensional spatial distribution of the ion current density and its cross section near the critical surface, produced by a 200-fs laser pulse of intensity 10^{16} W/cm^2.

In the work [A-05], the following issues have been analyzed: the influence of the plasma density scale length gradient (L_n) and the wavelength λ_L on the energy of the emitted protons E_i[keV] and the intensity of the proton beams I_i[W/cm^2] for the first and second harmonic of the Nd: YAG neodymium laser emitting 1ps pulses with a maximum intensity of $I_L = 10^{17}$W/cm^2. The optimal value of L_n/λ_L has been found, when the E_i and I_i reach maximum values (see Fig.8).
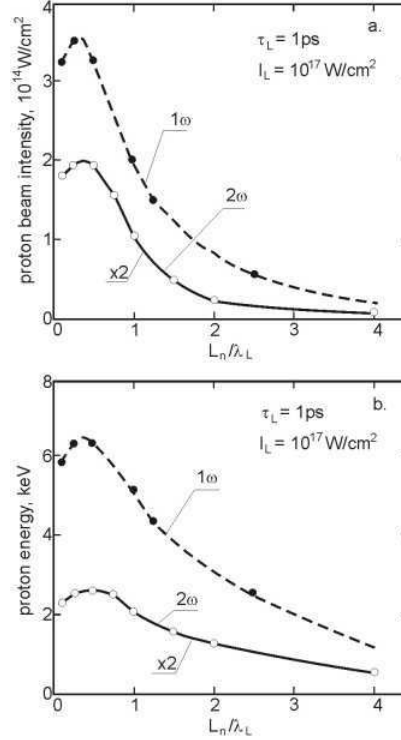

Fig.8 The effect of initial plasma density gradient scale length, L_n, on parameters of a forward-accelerated proton beam. 1 ω is the first harmonic and 2 ω is the second harmonic of Nd:glass laser.

In the case of forward acceleration, the best parameters are obtained for $L_n < \lambda_L$, for backward acceleration the most favorable conditions are obtained for $L_n > \lambda_L$. Presented numerical simulation results were confirmed by the experiments presented in the same paper. The experiment was performed with the use of 1-ps, 1.05-μm sub joule laser pulse generated by a terawatt CPA Nd:glass laser. A specific feature of the ps pulse was its temporal shape comprising the long-lasting (> 0.3 ns) low-intensity background and the short-lasting prepulse (a sequence of a few ps pulses covering the time period $\sim 10^{-10}$ s) of the intensity $\sim 10^4$ times lower than the intensity of the main ps pulse. As the intensity of the long-lasting background was at least 10^8 times lower than that of the main pulse, no preplasma was produced by it on the target surface. The short-lasting prepulse produced the preplasma of the thickness $L_{pre} \leq 5$ μm. This preplasma thickness was at least several times smaller than the laser focal spot diameter d_f, so the condition for the quasiplanar skin-layer interaction of the laser beam with the preplasma was fairly well fulfilled.

A significant effect associated with the processes of interaction of laser radiation with long density scale length L_n targets is the occurrence of rippling phenomenon involving local changes of density of electrons and ions under the influence of ponderomotive force, leading to the formation of so called von-Laue grating. Such self-generated grating prevents the propagation of laser radiation through the plasma and prevents energy deposition to the critical region of plasma. It leads to an ineffective laser acceleration. This effect was

investigated for relatively long laser pulse times ($\tau_L > 20$ ps), but there was no works devoted to shorter pulses that were relevant to the scope of research in the research team to which I belonged. In paper [A-06] I undertook the task of investigating this phenomenon and finding a remedy. Numerical studies were performed for beams with an intensity of $I_L = 10^{16}$-10^{18}W/cm^2, pulse length $\tau_L < 10$ ps, and wavelength $\lambda = 1.06$ μm. In my work, I studied the broad-band laser irradiation method (Deng 1986a, 1986b), when some waves with different frequency (from $0.5\omega_0$ to $2.0\omega_0$) pass through plasma simultaneously, instead of one frequency ω_0.

This treatment resulted in a significant reduction in the rippling effect. Using the three and five waveforms with changed frequencies, I managed to achieve a very good level of suppression of the above mentioned phenomenon. In the case of the three-wave method, the optimum variant of the quenching was obtained for $\Delta\omega = 0.5\%$, and for the five-wave model for $\Delta\omega = 1.0\%$ (Fig.9, Fig.10). In both cases rippling was suppressed three times relative to the case of one wave.
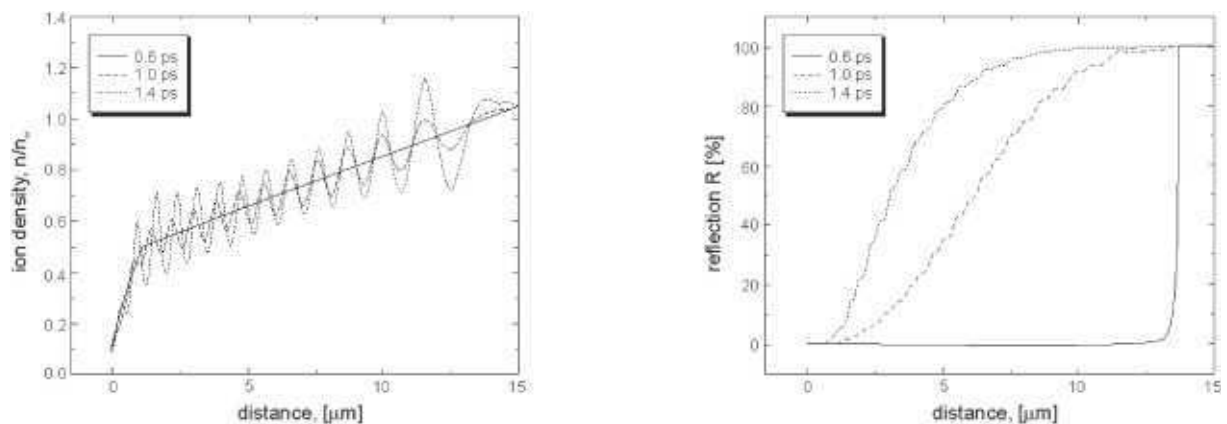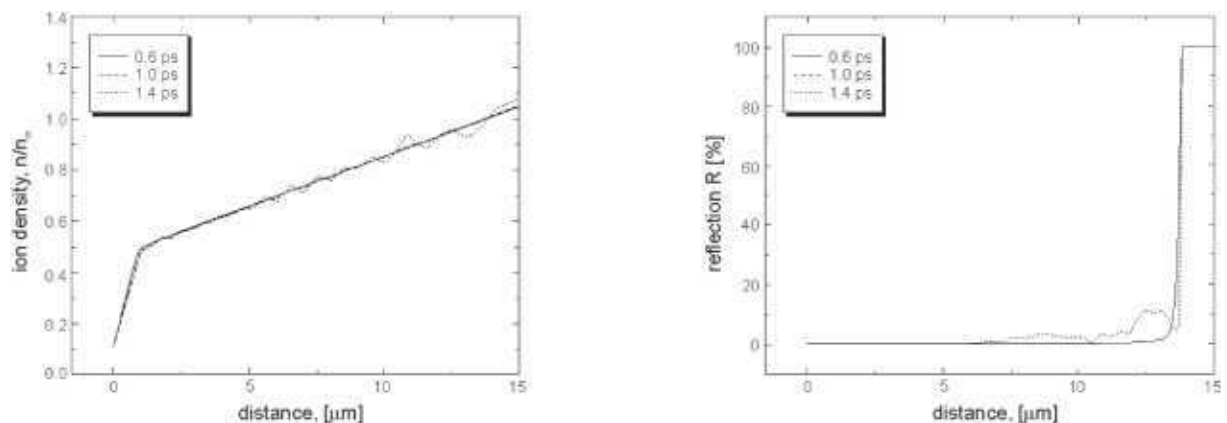

Fig.9 Evolution of ion density profile (left figure) and reflection of laser beam from plasma region (right figure) as a function of distance and interaction time for one wave. $I = 10^{16}$ W/cm^2, $\tau_L = 1$ps, $\lambda = 1.06$ μm.

Fig.10 Evolution of ion density profile (left figure) and reflection of laser beam from plasma region (right figure) as a function of distance and interaction time for five waves of $\Delta\omega = 1.0\%$ ω_0. $I = 10^{16}$ W/cm^2, $\tau_L = 1$ps, $\lambda = 1.06$ μm.

This work was supplemented by [A-08], which presents an analytical explanation of the rippling process and is confronted with the work [A-06]. This paper presented the analytical description of two processes dealing with the skin-layer ponderomotive acceleration method of fast ion generation by a short laser pulse: ion density rippling in the

underdense plasma region and generation of ion beams by trapped electromagnetic field in plasma. Starting from Maxwell's equations describing longitudinal fields acting between electrons and plasma ions in presence of standing electromagnetic waves, analytical solutions describing ponderomotive forces in the studied plasma area were determined. After calculating the mean values of electric fields, stationary solutions for electrons and ions were obtained. The results of the analytical solutions were compared with the simulation results and found to be well matched.

With the development of high-power laser systems, a new type of laser-target interaction has emerged. It is about the interaction of the relativistic type. For this purpose, a special, relativistic and hydrodynamic 2D code was created (2006). The code was useful for description of laser-target interactions for beams of intensity up to 10^{20}W/cm^2.

In the first approach, the aforementioned code was used in [A-07], where the dependence of the structure and angle of ion beam divergence as a function of the product d_L/L_n (where: d_L-laser beam diameter, L_n-plasma density scale length), was investigated.

As is well known, such fields of physics as high-energy-density physics HEDP, fast-ignition FI in inertial confinement fusion, and positron emission tomography PET require ion beams with the possible lowest divergences, moderate ion energies $E_i \leq 5$ MeV and high density ion currents $j_i > 10^{13}$W/cm^2. The simulation showed that for the case $d_L >> L_n$ ($d_L/L_n=32$) and $d_L \geq 5\lambda_L$ ion beams with small divergence ($\theta_i \leq 10°$) can be obtained, while for $d_L/L_n \leq 16$ the divergence of beams can reach up to 45° (Fig.11). The dependence of ion beam divergence on laser beam intensity for the case $d_L/L_n=32$ was weak (Fig.12).
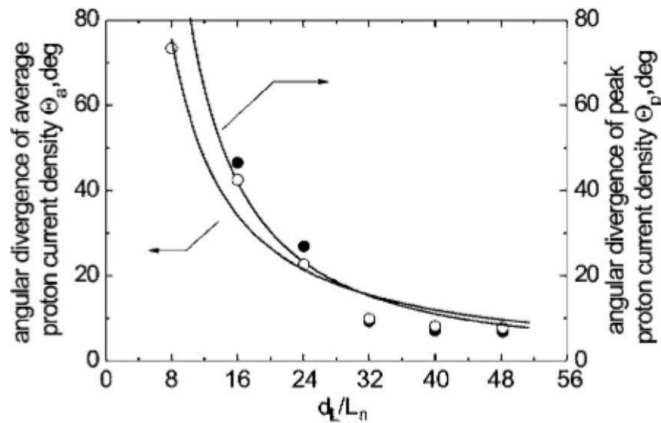

Fig.11 Dependence of angular divergence (FWHM) of the peak and the average proton current density on the ratio d_L/L_n at $d_L=20$ μm.
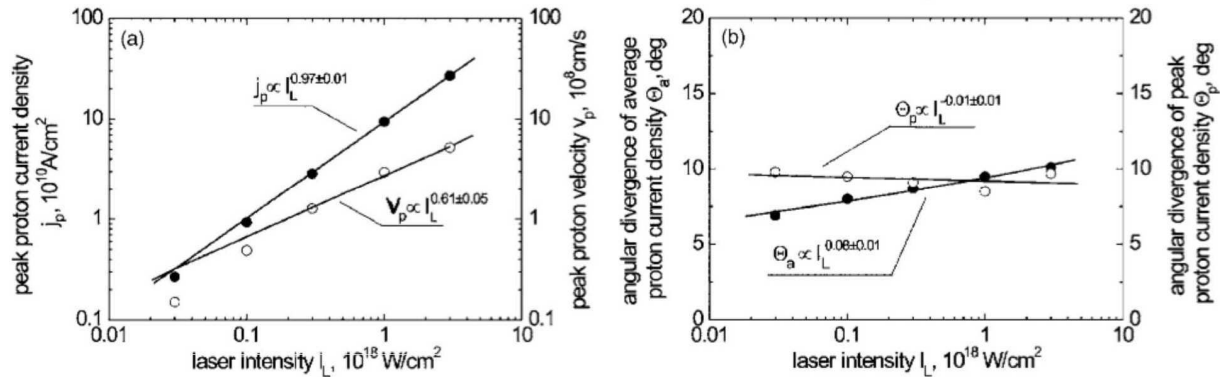

Fig.12 Dependence of proton beam parameters on laser intensity, for $d_L=20$ μm, $\tau_L=0.25$ ps, $L_n=0.625$ μm, t=196 fs.

The work [A-09] is devoted to the comparison of the efficiency of two basic ion beam generation methods, the TNSA and S-LPA method for their use as effective approaches for fast ignition (FI) in inertial fusion (ICF) experiments. It has been shown that S-LPA based proton acceleration give ion bunches with density approximately 1,000 times greater than in the case of TNSA acceleration. In the case of TNSA method and for the laser intensity $I_L = 5$ x 10^{19}W/cm^2, it is possible to obtain ion beam densities of 10^{19}cm^{-3}, meanwhile for fast ignition we need densities of order $n_i \geq 10^{22}$cm^{-3}. This means that in order to achieve the required level, one would have to focus the ion beam a thousand times, which can be a big challenge, especially since, in addition to low density, TNSA method produces divergent beams. In the case of S-LPA acceleration method, the required density of ion beams is obtained without focusing. Performed 2D simulations for the Gaussian beam with the parameters $\tau_L = 250$ fs, $I_L = 3$ x 10^{18}W/cm^2 led to obtaining ion beams (acceleration S-LPA) with the parameters: $n_i = 5$ x 10^{21}cm^{-3} (axis of symmetry of the target) $j_i = 3$ x 10^{11}A/cm^2, $I_i = 5$ x 10^{16}W/cm^2 and energies $\sim$ 150 keV. For numerical investigation, a target with preplasma thickness $L_{pre} = \sim 5$ μm was used. When the laser beam width $d_f \gg L_{pre}$ divergence of the resulting ion beam was small (Fig.13), $d_f = L_{pre}$ produced a complex structure responsible for an increased divergence of accelerated ions (Fig.14).
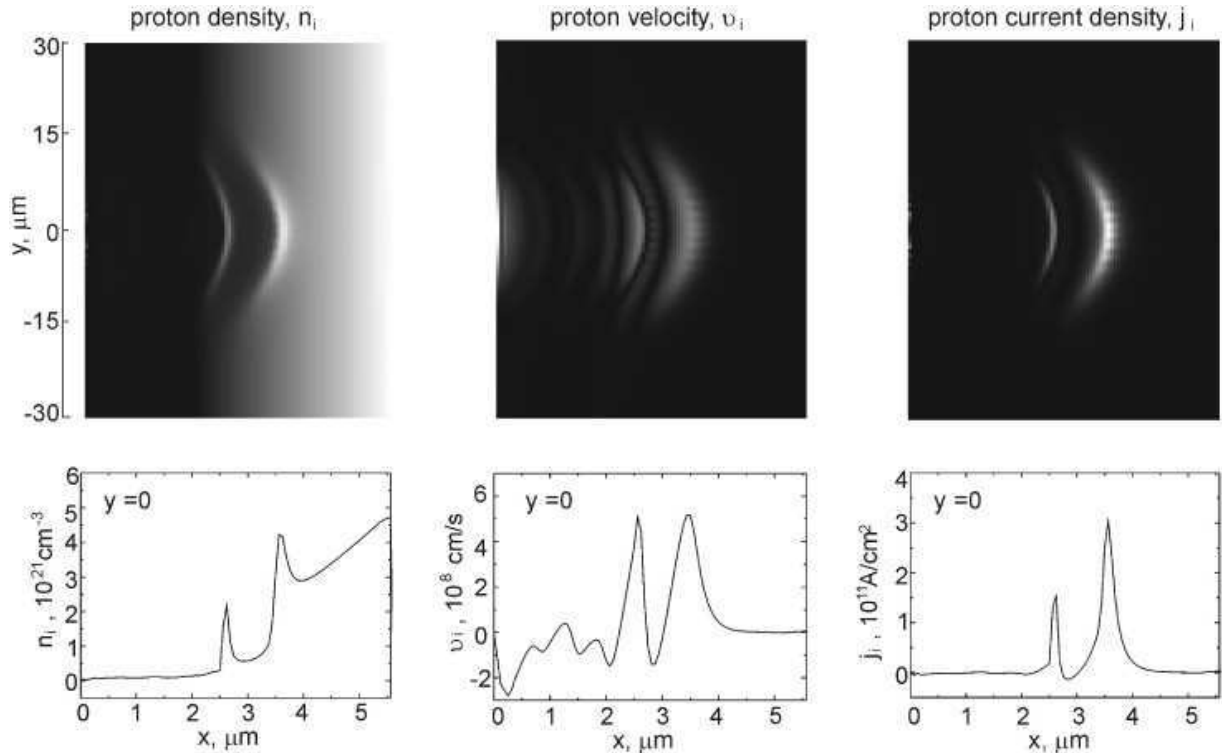

Fig. 13 Results of a numerical simulation of high-density plasma (proton) block generation
by S-LPA obtained with the use of 2D two-fluid relativistic hydrodynamic code.
The laser pulse of $\tau_L = 0.25$ ps, $\lambda_L = 1$ μm, $I_L = 3$ x 10^{18} W/cm^2 and $d_f = 20$ μm interacts
with hydrogen preplasma of 3 μm thickness at the critical density.
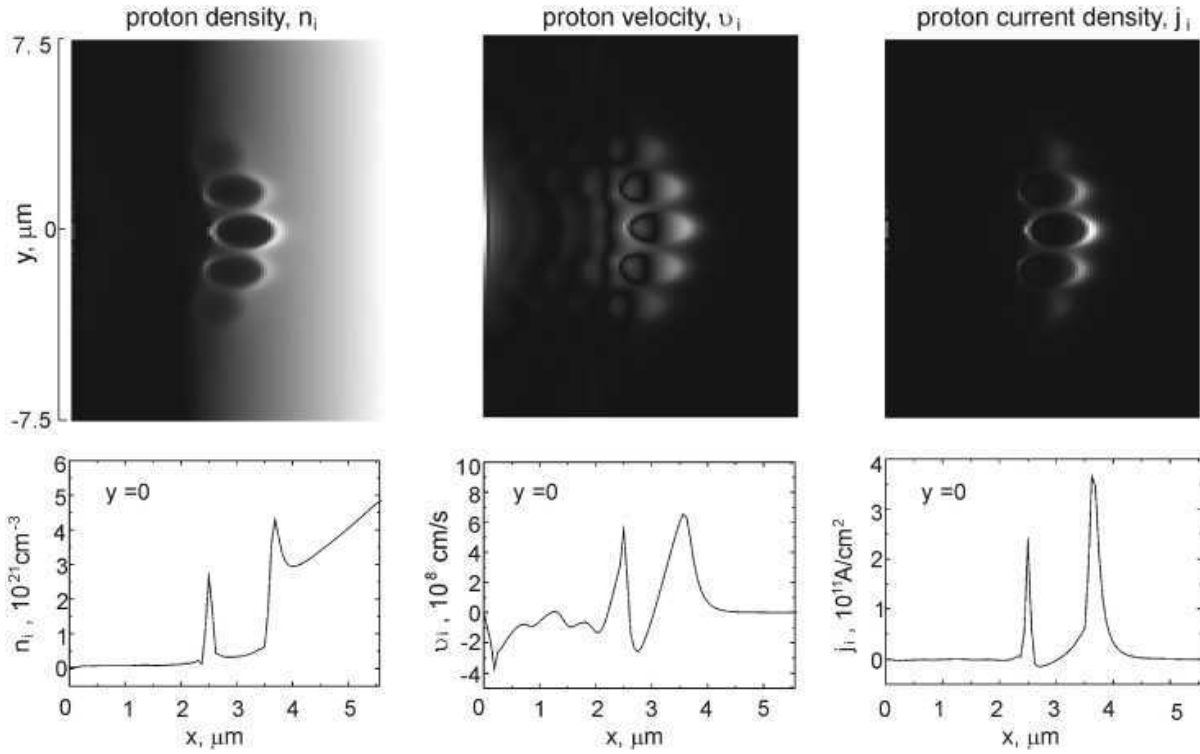
Fig.14 As in Figure 13 but at d_f =5μm.

In the article [A-10], investigations on the problem of ion beam divergence obtained during S-LPA acceleration, from [A-07] were extended. The study was focused on the correlation between the ion beams divergence and the laser beam parameters such like laser beam intensity ($I_L \geq 10^{17}$ W/cm^2) and beam widths as well as preplasma lengths. The aim of the study was to investigate the angular parameters of accelerated ion beams for relativistic cases ($I_L \geq 10^{17}$ W/cm^2) and to test whether relativistic conditions increase ion energy from hundreds of keV (subrelativistic) to the energy of the MeV. The research was numeric. It was found that in the case of the relativistic propulsion of hydrogen targets ($I_L = 3$ x 10^{18} W/cm^2), as well as for the subrelativistic cases described in [A-07], two regimes with strongly different pattern of angular distribution of ions are observed. For $L_n = 0.75\lambda_L$, $d_L/L_n = 27$, $d_L = 20$ μm (where: d_L- diameter of the laser beam, L_n-plasma density scale length) the beam divergence was small and comparable with the analogous sub-relativistic case, in the case of $d_L/L_n = 4$, $d_L = 3$ μm, as before, formation of bubbles in the preplasma led to a significant deterioration of the ion beam convergence (Fig.15).
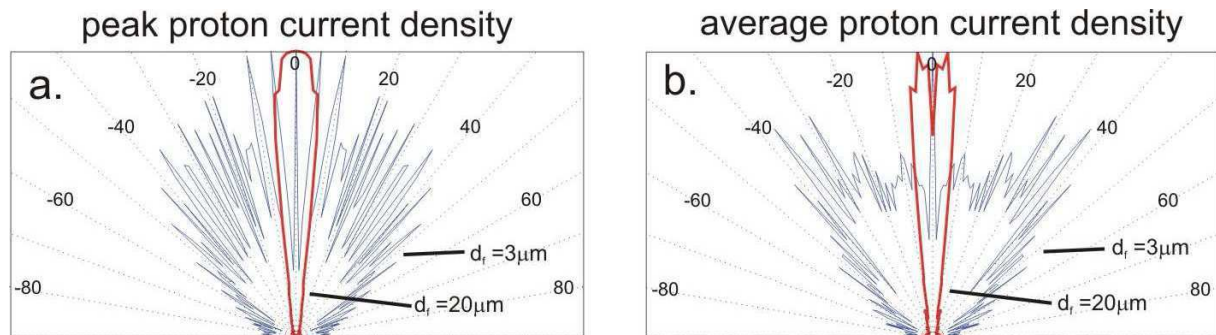

Fig.15 Angular distributions of proton current densities at $t = 196$ fs for $d_L = 3$ μm and $d_L = 20$ μm.

For $L_n = 2.5\lambda_L$ and $d_L = 20$ μm, the beam is also disturbed, which is explained by the self-focusing effect of the laser beam leading to the generation of the standing wave in the plasma subcritical region and, consequently, the formation of a bubble structure leading to increased divergence. In summary, it is stated that for $d_L \gg L_n$ (say $d_L > 30L_n$) and $d_L > 5\lambda_L$, the difference in ion beam Θ_i is small for both subrelativistic and relativistic acceleration cases, and, in addition, for the second case of commercial lasers 100TW/10kHz a multi-MA proton beam can be obtained with a current density of TA/cm^2.

Using a two-dimensional (2D) relativistic hydrodynamic code, it has been shown that it is possible to obtain effective focusing of high current density ion beams using profiled, curved targets [A-11]. It has been shown that the parameters of beams obtained in this way strongly depend on the density gradient scale length (L_n) and the radius of curvature of the target R_T. When $L_n \leq 0.5\lambda_L$ (λ_L -wavelength of laser) and R_T is comparable to a laser beam aperture d_L then a significant portion of accelerated ions may be concentrated on an area much smaller than d_L which results in a significant increase in fluence and current density. It has also been demonstrated that using picosecond, multipetawatt laser that generate relativistic pulses $I_L \sim 10^{20}$W/cm^2, will be able to obtain ion beams with parameters close to those required for the fast fuel ignition DT, during the focusing process. In general, a decrease in the fluence value F_i, current density and efficiency of the ion beam was observed with the increase in the R_T/d_L ratio. For $d_L=R_T=40$μm, $L_n \approx 0.7\lambda_L$, $I_L = 3 \times 10^{18}$W/cm^2 and $\tau_L = 0.25$ ps the relative increase in fluence was equal to $g_F \approx 13$ and the relative increase of average current density was equal to $g_j \approx 35$. For the 3D case, the predicted increase of these values should be: $g_F > 10^2$ and the average current density $g_j \approx 10^3$ (Fig.16).
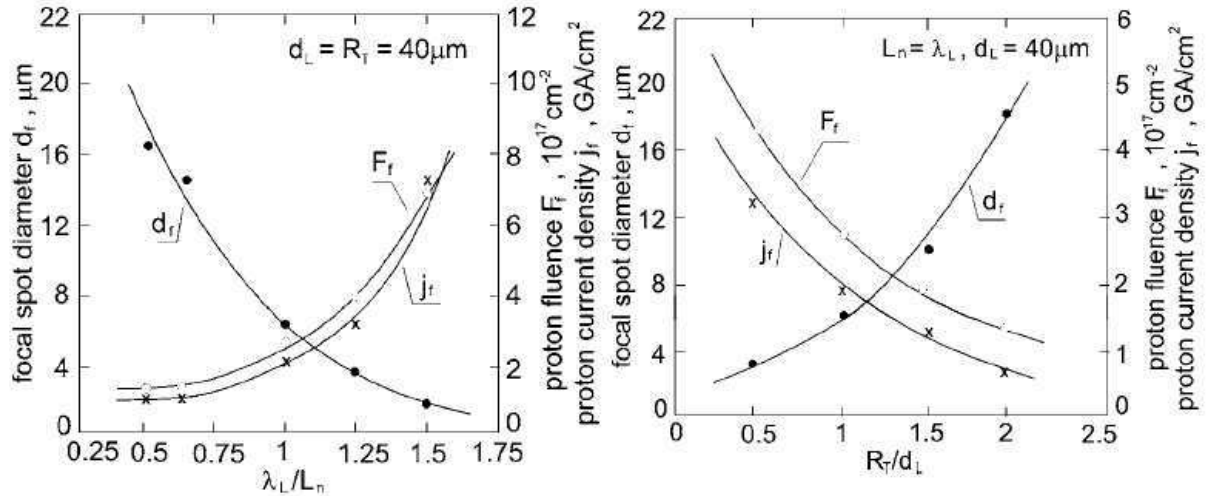

Fig.16 Dependence of proton beam parameters in the focal plane, $x = x_f$, on the preplasma density gradient scale length (left figure), on the radius of curvature of the target front surface (right figure). $I_L = 3 \times 10^{18}$W/cm^2.

In [A-12], anomalous observations using the fast ignition for laser driven fusion energy are interpreted and experimental and theoretical results are reported which are in contrast to the very numerous effects usually observed at petawatt-picosecond laser interaction with plasmas. These anomalous mechanisms result in rather thin blocks (pistons) of these nonlinear (ponderomotive) force driven highly directed plasmas of modest temperatures. The blocks consist of space charge neutral plasmas with ion current densities above 10^{10} A/cm^2. For the needs of applications in laser driven fusion energy, much thicker blocks are required. This may be reached by a spherical configuration where a conical

propagation may lead to thick blocks for interaction with targets. First results are reported in view of applications for the proton fast igniter and other laser-fusion energy schemes.

In the publication, among others, both plasma and preplasma density changes observed during the interaction of 4 ps pulse of the Nd:glass laser with the target made of deuterium were analyzed (Fig.17). Additionally, evaluation of angular distribution of Au ions beam, depending on the pulse length, was made (Fig.18).
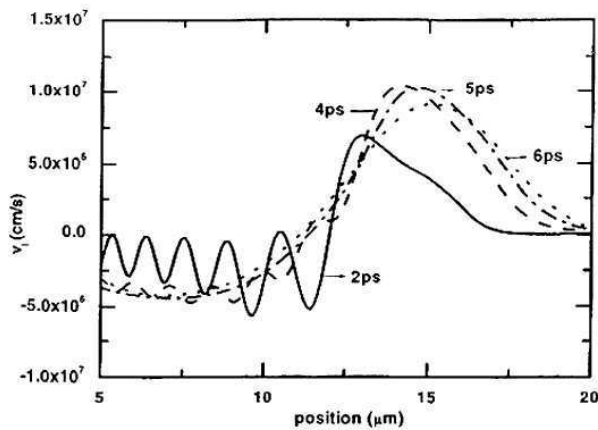

Fig.17 Ion velocities computed for a one-dimensional $3*10^{15}$ W/cm² neodymium glass 4 ps laser pulse at some different times.
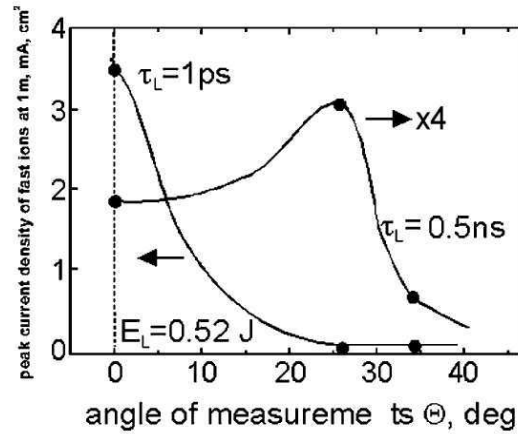
Fig.18 Measured value of the peak current density in the function of ion emission direction for different pulse length.

The authors conclude that using laser plasma acceleration it is possible to produce ion blocks with high values of current density ($j_i > 10^{10}$A / cm²), characterized by high directionality (short pulses $\tau_L \sim$ 1ps) and large thicknesses (acceleration of curved targets in conical cavities), which allows the use of this method of accelerating as an efficient way in the fast ignition procedure.

In the extensive work [A-13] a detailed evaluation and review of the current state of research (for year 2007) on the fast ignition project (FI-fast ignition) carried out with the use of electron beams and ion beams produced with the use of high-powered lasers was conducted in a comprehensive manner and the prognosis regarding research development in this field were made. This method consists in introducing into the pre-compressed DT fuel target (compressed up to a value of approx. 300 g/cm³) electrons or ions beam with specially selected parameters in order to initialize the ignition. At the beginning, the parameters that the ion or electron beam must meet are discussed, so that it can be used as an igniter of the pre-compressed spherical DT fuel with a density of ρ = 300 g/cm³.

The required parameters were: $E_{ig} \approx$ 17 kJ, $I_{ig} \approx 7 \times 10^{19}$Wcm⁻², $\tau_{ig} \approx$ 20 ps, $r_{ig} \approx$ 20 μm (where E_{ig} - ion beam energy, I_{ig} - ion beam intensity, τ_{ig} - ion pulse length and r_{ig} - ion beam beam). A relation was presented that allows to calculate the optimal value of the laser pulse intensity enabling the formation of such ion beams. The essence of the problem related to the efficiency of deposition of laser energy to ionic targets was indicated (in normal acceleration conditions, this efficiency <10%). Fig.19 presents the dependence of the efficiency of energy transfer from a laser to protons and the intensity of proton beams in the place of their creation as a function of laser intensity.
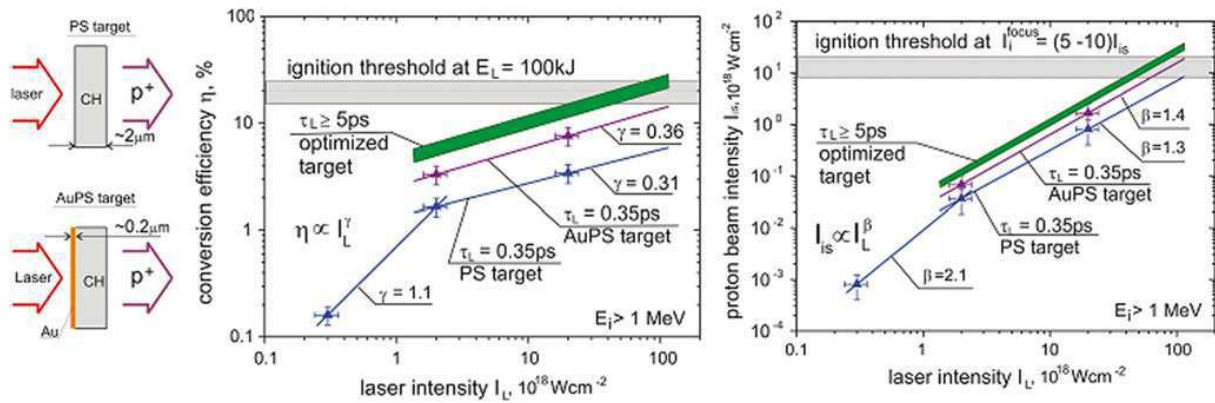
Fig.19 The laser-MeV protons energy conversion efficiency and the MeV proton beam intensity at the source (close to the target) as a function of laser intensity for PS and AuPS targets.

In the paper, the concepts of the implementation of effective ion acceleration processes based on the methods used in the world and own research (experiments on the LULI system, numerical simulations) were presented (Fig.20).
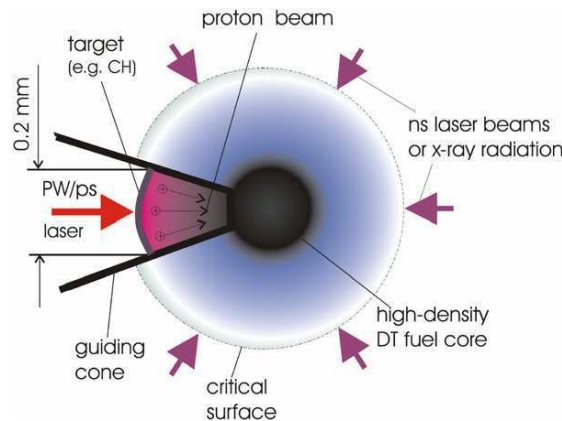
Rys.20 The concept of FI with SLPA-produced proton beam. A dense focused proton bunch (plasma block) generated at the interaction of a PW laser with a dielectric hydrogen-rich target of the curved front surface ignites the DT fuel compressed by cone-guided implosion.

At the end, existing and designed laser systems from around the world were presented, including: Japan - FIREX I, GEKKO XII, United States - OMEGA, HEPW, SNL, NIF, China - SG-II, Europe - Vulcan PW, Petal and Hiper.

In summary, FI has significant advantages over the classical ICF method based on pure single stage DT fuel compression up to a value of over 600 g/cm^3. FI, as it results from numerical tests, can be implemented even at the physically achievable parameters of laser beams, i.e. EL <100kJ energy, on multi-kJ, PW laser systems planned or existing in 2007.

In the years 2007-2008 I worked on relativistic, one-dimensional particle-in-cell (PIC) code. This type of codes are considered to be Lagrange-Euler kinetic codes, which in general deal with collisionless plasmas. The advantage of such codes is that they are ideally suited to investigate the effects of relativistic intensity of laser radiation with plasma for which the hydrodynamic approach loses its physical meaning. The generated code was an analog of the well-known LPIC++ code used successfully in simulation work. Within the framework of the code, it was possible to profile preplasma and postplasmas (linear and exponential profiles), linear and circular polarization simulation, as well as modeling of C_nH_n composite targets

(two-component targets made of plastics such as PS, CH), metal targets with occluded proton layer and single component targets.

As a result of the studies described in [A-14, A-15], the proton emission from thin solid targets (1 - 3 μm) subjected to 0.35 ps laser pulse, derived from laser beam of energy 15 J, concentrated to give the intensity $I_L = 2 \times 10^{19} W/cm^2$ was analyzed. It has been shown that, under conditions of S-LPA protons acceleration regime, we can produce beams of terawatts power and intensities up to $10^{18} W/cm^2$. It has also been noted that the parameters of the resulting beams depend significantly on the structure of the target and can be significantly improved by the use of Au/PS double-layer targets (Au 0.1 - 0.2 μm shield coated with polystyrene). The work was based on the results obtained on a laser 100 TW LULI for wavelength $\lambda_L = 1.05$ μm, pulse length $\tau_L = 350$ fs and contrast ratio ~ 10^7. In the course of the experiments PS polystyrene targets (1 - 3 μm) and double layer Au/PS targets (Au 0.05 - 0.2 μm target coated with polystyrene) were tested. In addition, the results of 1D simulations were performed using relativistic, particle-in-cell (PIC) code created during this period. In conclusion, the obtained results give real hope for improving the intensity of proton beams that can be used in the fast-ignition (FI) process (Fig.21).
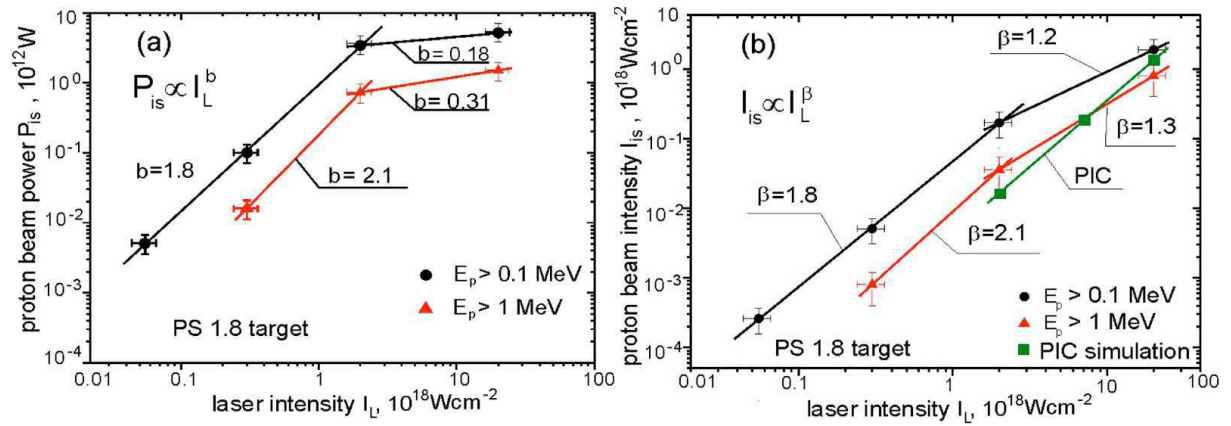

Fig.21 The (a) proton beam power and (b) intensity at the source as a function of laser intensity. Points with error bars—the results of IC measurements; lines—the results of approximation by a power function. Points without error bars—the results of PIC simulations, in which a super-Gaussian 0.35 ps laser pulse interacted with an inhomogeneous hydrogen plasma layer.

An important parameter for proton beam acceleration is the wavelength of laser radiation used in this process. The influence of this parameter on the properties of the generated beams was investigated in [A-16]. The research was numeric. Using its own PIC 1D numerical code, acceleration was measured for the first 1ω, the second 2ω and the third 3ω harmonic of the Nd:YAG laser and the pulse duration $\tau_L \leq 1$ ps. The laser beam was polarized linearly and the thickness of the test targets varied between 0.1μm and 8μm. Preplasma had exponential profile. The maximum concentration of protons was equal to $n_{max} = 4 \times 10^{22}$ cm^{-3} for solid polyethylene targets (CH) and 10^{23} cm^{-3} for polystyrene targets (CH$_2$). In the course of the simulation, it was established that for the laser wavelength decreasion and for the constant value of product $I_L\lambda^2$, the contribution of the S-LPA mechanism to the proton acceleration had been increased, which made almost all ion beam parameters (ion beam intensity, current density, energy fluence and average as well as maximum energy of the ions) increase as well. Even with moderate values of $I_L\lambda^2 \leq 10^{20} W$ cm^{-2} μm^2 and for short wavelengths ($\lambda \leq 0.5$ μm), it is possible to obtain ultrashort (≤ 100 fs), multi-MeV proton beams with intensities and currents reaching of 10^{21} W/cm^2 and 10^{14} A/cm^2

(Fig.22). In particular, the use of a multipicosecond shortwave laser source (eg 2ω, 3ω Nd: YAG laser), with circular polarization, appears to be a promising and high-efficient ($\eta \geq 15 \%$) method for proton beams production with parameters required for realization of fast ignition FI.
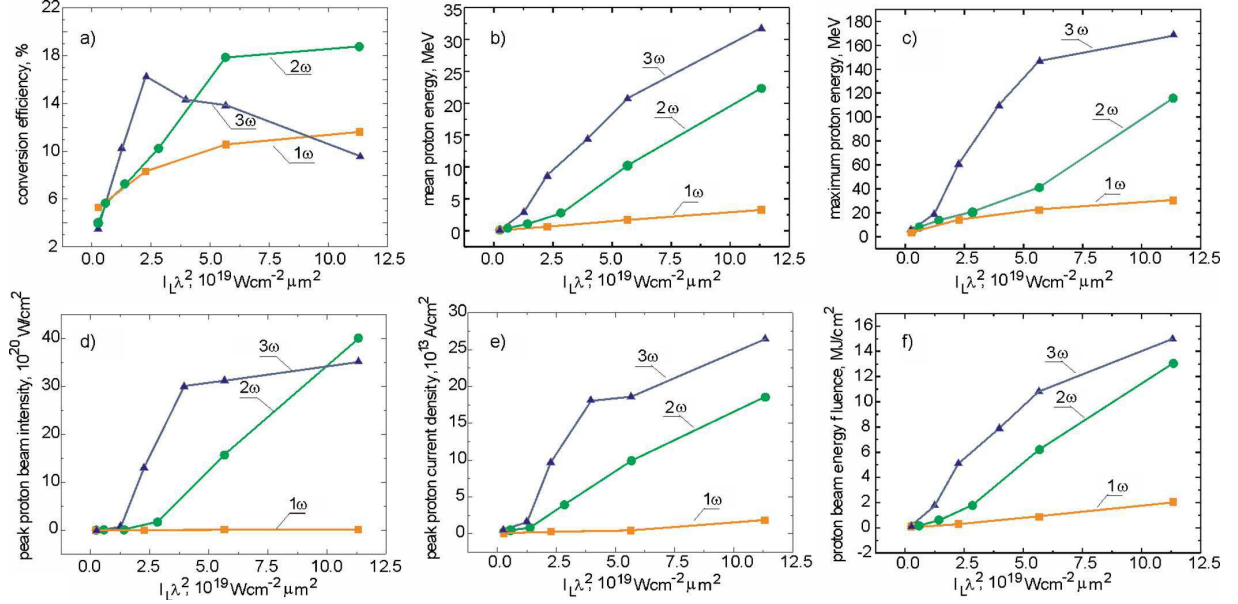

Fig.22 Parameters of proton beams driven by laser pulses of different wavelengths (corresponding to the 1ω, 2ω, and 3ω beams of Nd:glass laser) as a function of $I_L\lambda^2$. L_T=1 μm, L_n=0.25 μm, τ_L=0.35 ps, and n_{max}=4 x 10^{22} cm^{-3}.

The results of the work described in [A-16] and their comparison with the results of experiments were investigated in paper [A-17], which analyzed the effect of intensity (I_L), wavelength (λ), target thickness (L_T) and preplasma gradient scale-length L_n) on the parameters of the produced proton beams, and the efficiency of energy transport from laser to ions (η). The results were compared with the results obtained in the experiments conducted on the 100 TW LULI laser, generating beam intensity I_L up to 2 x 10^{19} W/cm^2. The calculations were carried out for laser pulses corresponding to the first (1ω) and second (2ω) harmonics of the Nd:glass laser, with the pulse duration τ_L from 0.35 ps to 2 ps and for the intensities I_L to 5 x 10^{20} W/cm^2. Except for the laser-protons energy conversion coefficient (η), where values were similar, for all remaining ion beam parameters, the acceleration advantage by the use of second harmonics pulse (2ω), over acceleration with the use of first harmonics pulse (1ω) was observed. In particular for the short preplasma, characterized by the so-called density gradient scale length L_n, the difference was the most observable. For $I_L\lambda^2 \geq 5$ x 10^{19} Wcm^{-2}μm^2, the peak intensity of the proton beam as well as the peak value of current density for case 2ω reached values: 10^{21} W/cm^2 and 10^{14} A/cm^2. In the part of the work devoted to the experiment with the use of 100 TW LULI laser enabling the generation of 0.35 ps pulses with a contrast of ~ 10^7 (1ω) and 10^8 (2ω) and with intensities up to 2 x 10^{19} W/cm^2, the laser beam interaction with polystyrene targets (PS) with thicknesses 0.6 - 1.0 μm was tested. In both cases (numerical and experimental) it was shown that the second harmonic (2ω) pulses of the Ng: glass laser generate proton beams with much higher intensities, current densities and energy fluence than is the case of 1ω pulses (Fig.23). Even with a moderate value of $I_L\lambda^2 \geq 0.5$ x 10^{20} Wcm^{-2}μm^2 for the picosecond pulses 2ω, it is possible to produce multi-MeV proton beams of an intensity of about 10^{21} W/cm^2 and current density of 10^{14} A/cm^2.
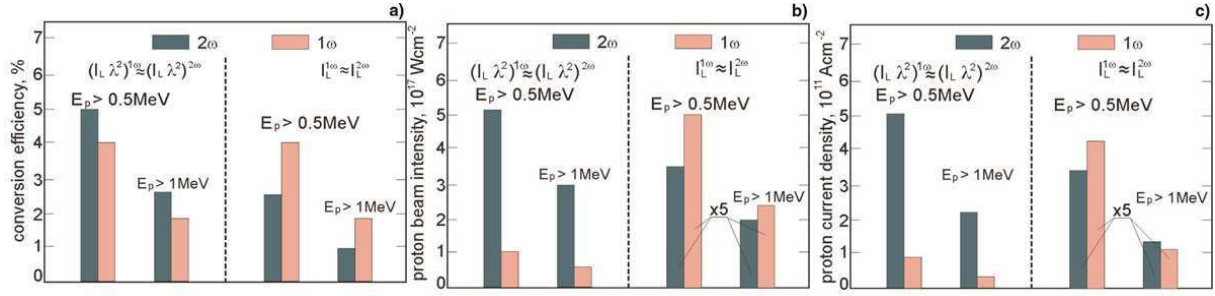
Fig.23 A comparison of laser-proton conversion efficiencies (a) as well as proton beam intensities (b) and current densities (c) at the source for moderate-energy (<3 MeV) protons generated by the 1ω or 2ω Nd:glass laser beam. The results obtained from the experiment at $I_L\lambda^2 \approx 2.1 \times 10^{18} Wcm^{-2}\mu m^2$, τ_L= 0.35 ps, L_T= 1 μm.

The low L_n value and lower wavelength leads to the preference of the S-LPA (RPA) over other acceleration types and to an increase in the laser-to-ions energy conversion ratio η > 10% and allows for significantly more intensive interaction with the thick targets than in the case of when first harmonic (1ω) of the laser for ion beams generation was in use. In addition, the higher contrast acceleration of 2ω reduces the heterogeneity of the generated beams, which increases their chance of being used in the fast ignition process during inertial confinement fusion (FI ICF).

The issue of acceleration to ultra-high velocity plasma projectiles with densities of a solid has become the basis for numerical studies described in the article [A-18]. The paper shows that with the use of picosecond pulses from ultraviolet (UV) lasers, it is possible to generate ionic projectiles with energy fluence of $F_i \geq 1$ GJ/cm^2 and subrelativistic velocities even for the moderate values of dimensionless laser amplitude $a_0 \sim 10$. The acceleration efficiency with the use of UV lasers is significantly higher than in the case of lasers with a longer wavelength (λ ~ 1 μm) and the same value of a_0. The propulsion of ion projectiles carried out on this principle is quite well described by the so-called "Light Sail" model. During the research, it was demonstrated that for circular polarization and pulse length τ_L=2 ps, the parameters of plasma projectiles depend significantly on the wavelength (test for λ=1.06 μm Nd: YAG and λ = 0.248 μm KrF). Thin targets with thickness L_T = 10 μm, preplasma gradient scale-length L_n = 0.25 μm, and concentrations of electrons and ions of 10^{23} cm^{-3} were tested. The assumed value of $I_L\lambda^2$ was 4 x 10^{20} Wcm$^{-2}\mu$m^2. In the first stage of acceleration, almost all ions and electrons are compressed to a value higher than the solid density (> 10^{23}cm^{-3}), and then such structure was accelerated to high speeds (v ~ 10^{10} cm/s) and high energy fluence > 1 GJ/cm^2. In addition, the dependence of conversion factor (η) and ionic energy (F_i) on function of $I_L\lambda^2$ was investigated.

It has been found that for the $I_L\lambda^2$ range from 0.25 x 10^{20} Wcm$^{-2}\mu$m^2 to 4 x 10^{20} Wcm$^2\mu$m^2, the conversion factor for the KrF laser is 5-6 times greater than for the Nd: YAG laser, and the energy fluence F_i is over 100 times higher for the former laser. For the $I_L\lambda^2$ = 1.5 x 10^{20} Wcm$^{-2}\mu$m^2 corresponding to $a_0 \sim 10.5$ conversion factor, the energy fluence and the average ion velocity for the KrF laser reach respectively: η ≈ 20 %, $F_i \approx$ 1GJ/cm^2, v ≈ 8 x 10^9cm/s (Fig.24). These parameters can be achieved for lasers with energies of ~ 100 kJ and they are sufficient for ignition of highly compressed DT fuel.
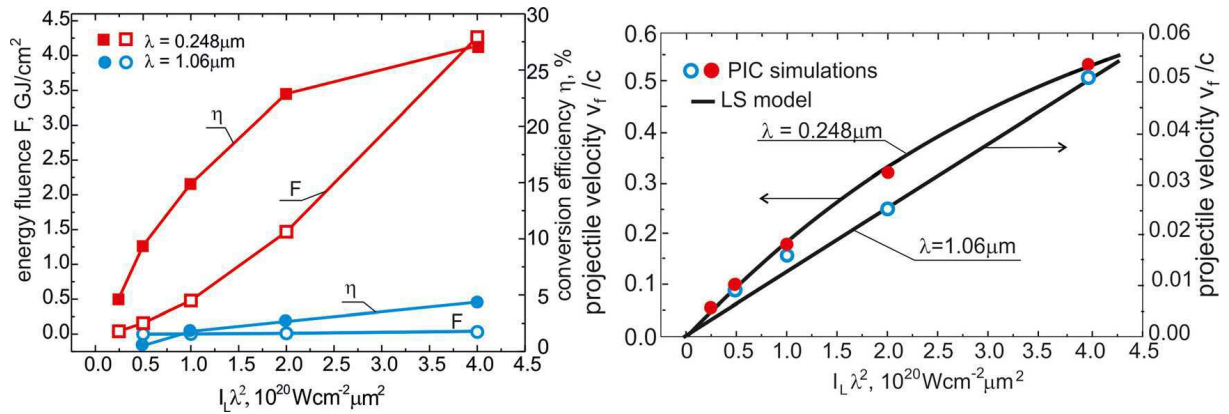
Fig.24 (Left image) The projectile energy fluence and the laser-projectile energy conversion
efficiency as a function of $I_L\lambda^2$ for KrF and Nd:glass laser driver.
(Right image) The final projectile velocity as a function of $I_L\lambda^2$ determined from the
LS model (solid lines) and the PIC simulations (dots and circles) for KrF and Nd:glass
laser driver.

In the years 2011-2012, the concept of a method for significantly improving the
efficiency of laser-ion energy transfer (η) and thus the parameters of the produced ion beams
was developed. This method was called acceleration using laser-induced cavity pressure
acceleration (LICPA). The method consists in placing the target inside a special, cylindrical
cavity to which a laser beam is inserted through a small hole. The beam inserted in this way is
trapped in the space between the accelerated target and the walls of the cavity. As a result of
reflections, the laser radiation enters into interaction with the target many times and its energy
is used much more effectively.

In [A-19], the analysis of the idea in two ways was undertaken. In the first approach,
using the 1kJ PALS laser system in Prague, LICPA acceleration under the hydrodynamic
regime was tested. Laser pulses of length 300 ps and wavelength 1ω ($\lambda = 1.315$ μm) as well
as 3ω ($\lambda = 0.438$ μm) with intensities I_L from 2×10^{14} W/cm^2 to 5×10^{15} W/cm^2 were
introduced into the reaction cavity. The experiment examined the size of craters made in
massive aluminum targets placed at the end of the cavity.

Under the influence of laser beams, targets made of polyethylene (10, 20, 30 μm CH),
polystyrene (6, 10, 20, 30, 50 μm PS) and aluminum (75 μm Al) coated with a mylar (2.5 μm)
or polystyrene (5 μm PS) were accelerated. The reaction cavities had the shape of a cylinder
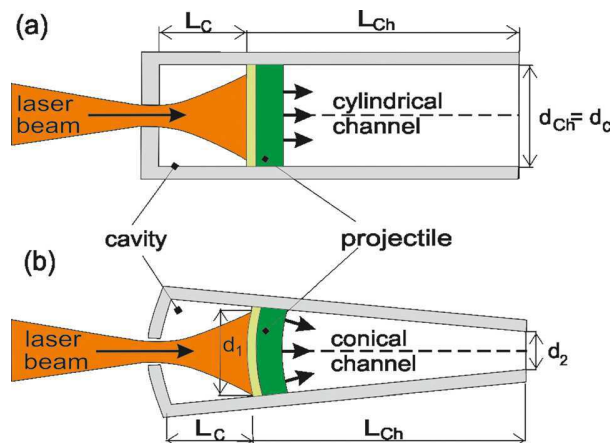or a cone (Fig.25).

Fig.25 Two geometries of laser-driven accelerators of dense matter using LICPA:
(a) the cylindrical accelerator and (b) the conical accelerator.

The results of comparison of the LICPA acceleration compared to the classic ablation drive (AA) indicate that the volumes of craters formed were more than an order of magnitude higher for the LICPA method than for the AA method (20 times for 3ω and 100 times for 1ω). This effect is explained by the fact that in the case of a forward moving projectile driven by the use of AA, only ~ 10% of the laser energy is deposited to its kinetic energy, while the rest of the energy is absorbed by the ablation layer moving backwards. In the case of the LICPA scheme, the energy of the ablation layer is recovered inside the cavity and converted into the energy of the driven projectile. In addition, much higher densities of projectiles and their velocities reaching ~ 2 x 10^7 cm/s were obtained for LICPA. The energy conversion efficiency η for the AA method is: ~ 4.4% (1ω), ~ 10.6% (3ω), and for LICPA 70% - 80% for 1ω and 3ω.

In the second approach, numerical tests of LICPA acceleration in the photon pressure acceleration regime, were carried out. Using of 1D PIC simulation, were investigated H^+, Be^{4+}, C^{6+} and Al^{13+} targets with assumption of realistic and constant surface density equal to $\sigma_h = \rho*L_T = 4$ x 10^{-4} g/cm^2. The laser beam used in the calculations was characterized by parameters: $\lambda = 1.06$ μm, $I_L = 2.5$ x 10^{21} W/cm^2, $\tau_L = 2$ ps (this corresponds to a beam diameter of 50 μm, 50 PW laser with 100 kJ energy). The length of the cavity ranged from 40 μm to 160 μm. The coefficient of reflection from the walls of the cavity $R_c = 0.64$ (1/3 of the energy reflected from the target during each cycle was lost as a result of imperfections of the walls and escape through the inlet opening of the cavity). As a result of the simulation, it was found that the LICPA method makes it possible to obtain neutral plasma projectiles with relatively narrow energy spectra propagating with subrelativistic velocities $v_p \sim 10^{10}$ cm/s. For fixed values of surface density of targets, such parameters of ion beams as: average energy per nucleon, fluence of kinetic energy F_i and the energy transfer coefficient from lasers to target are practically independent of ion type (Fig.26). Parameters of proton beams had values: $Fp \sim 2$GJ/cm^2, $I_p \sim 10^{22}$ W/cm^2, $j_p \sim 10^{14}$ A/cm^2, $\tau_p <$1ps. Energy conversion efficiency η reaches a level of 60 - 70%. All these values are significantly higher than in the case of pure RPA (without a cavity) drive, which means that these beams can be successfully used in the fast ignition (FI) of inertial confinement (ICF).
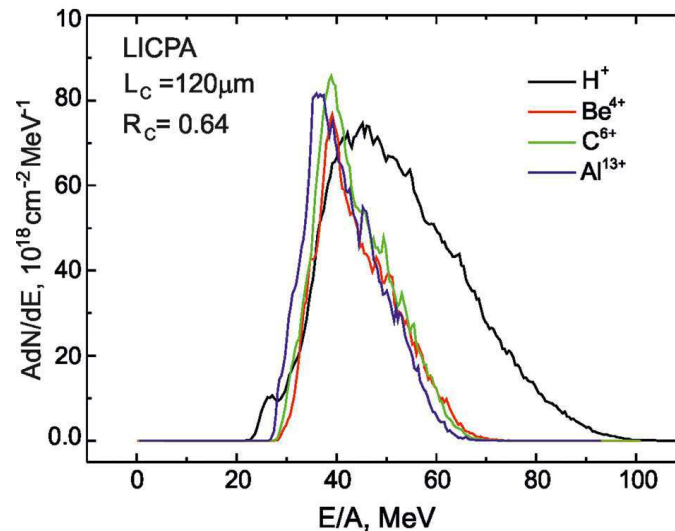

Fig.26 The ion energy spectra of plasma projectiles of various kinds of ions accelerated in the photon pressure-driven LICPA accelerator. For all kinds of ions, $\sigma_h = \rho_L L_T = 4$ x 10^{-4} g/cm^2 and L_T (Al^{13+}) = 1.48 μm, L_T (C^{6+}) = 2 μm, L_T (B^{4+}) = 2.16 μm, L_T (H^+) = 28.6 μm.

The research described in the article [A-20] was an attempt to determine the advantages in the acceleration of ionic carbon targets using the LICPA method in relation to the acceleration using the classic method of RPA (radiation pressure acceleration). Based on the PIC 1D simulations, the case of acceleration of carbon targets using laser picosecond pulses with circular polarization and intensity of $\sim 10^{21}$ W/cm^2 for the LICPA and RPA methods was investigated. In the calculations, it was assumed that the carbon target had a thickness of 2 μm to 8 μm and a starting concentration of $n = 10^{23}$ cm^{-3} and the density gradient scale-length $L_n = 0.25$ μm. The impulse and the laser beam were characterized by the following parameters: $I_L = 2.5$ x 10^{21} W/cm^2, 5 x 10^{21} W/cm^2, 8 x 10^{21} W/cm^2, $\tau_L = 2$ ps. The cavity length was of 40 μm to 160 μm, and the reflection from the walls had the value of $R_c = 0.64$. It has been shown that the use of different lengths of cavities does not lead to the widening of energy spectra, which means that despite the multiple reflection of the beam inside the cavity does not spoil the acceleration process. At the same time, the comparison of the shapes of energy spectra obtained as a result of driving with beams of different intensities $I_L = 2.5$ x 10^{21} W/cm^2, 5 x 10^{21} W/cm^2 proves that the relative width of the spectrum remains unchanged (Fig.27).
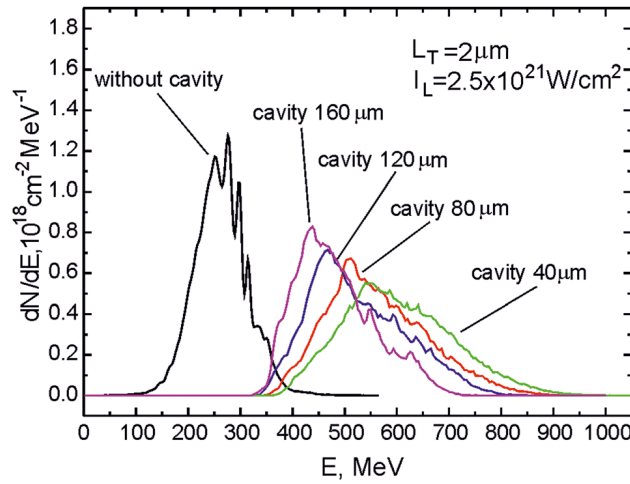

Fig.27 Energy spectra of carbon ions accelerated in the LICPA scheme (with the cavity length L_c varying from 40 μm to 160 μm) or in the RPA scheme (without the cavity). $L_T = 2$ μm, $I_L = 2.5$ x 10^{21} cm^2, $R_c = 0.64$, $l_{acc} = 150$ μm.
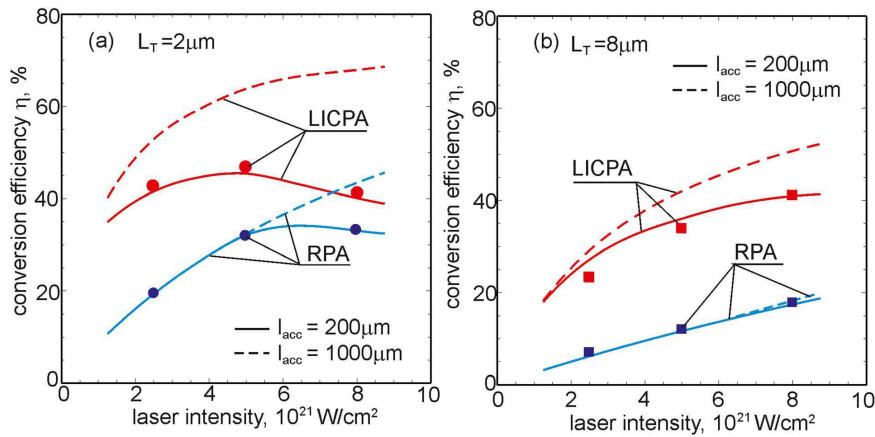

Fig.28 The laser-ions energy conversion efficiency in the LICPA scheme and the conventional RPA scheme. Solid and dashed lines denote the GLS model predictions. Circular and square dots denote results of the PIC simulations. $L_c = 120$ μm or ∞, $R_c = 0.64$.

In addition, there is a significant improvement in the energy conversion coefficient η for the LICPA scheme in relation to the RPA scheme and this is an improvement of the order of 2.

In the case of thin targets (2 μm), a faster and larger conversion efficiency increase is observed along with an increase in the intensity of the laser beam, reaching 45% for I_L = 2.5 x 10^{21} W/cm^2, compared to thicker targets (8 μm), where we have a maximum of 32% for the same intensity (Fig.28).

However, for thin targets in the higher I_L region, the target can be penetrated and disrupted by strong laser pulse, which stops the further improvement of the laser-target energy transfer coefficient η. In summary, however, it should be emphasized that using picosecond lasers with intensities of ~ 10^{21} W/cm^2 LICPA can generate carbon Ions with sub-GeV to multi-GeV energies with energy fluence ≥ 1 GJ/cm^2 and beam intensity > 10^{20}W/cm^2. All these features testify to the usefulness of the discussed method for the production of ion beams in the physics of high power density (HEDP) and inertial fusion (ICF).

In the years 2012-2013 I built a relativistic particle-in-cell (PIC) 2D code named PIC2D, which allows analyzing many issues related to the interaction of laser beams with ionic targets unreachable in the 1D code. The code enabled the analysis of realistic shapes of laser beams with regard to their spatial dimensions and such phenomena as divergence or convergence. It was possible to follow the real structure of electromagnetic fields and spatial distributions of ions and electrons. The program allowed for simulation of LICPA acceleration conditions taking into account the shapes of the cavity (cylindrical cavity or conical cavity), variable inlet opening size and real cavity walls (e.g. modeling walls made of gold Au). In the case of LICPA 2D simulations, it was possible to resign from the arbitrary selection of the loss factor R_c, which was characteristic of the 1D calculations. The result of this work was the paper [A-21], in which the physical and numerical bases of 2D code were presented, as well as preliminary results of calculations made on the basis of the discussed program. As mentioned before, the PIC2D code is fully relativistic (electrons and ions) that combine Maxwell's equations, describing electromagnetic fields, with relativistic equations for the so-called macroparticles representing large sets of electrons and ions. The code from the numeric side belongs to the so-called Lagrange and Euler codes. Electric and magnetic fields, current densities as well as concentrations of electrons and ions are counted in immobile Euler mesh nodes (these meshes are specially shifted relative to each other) (Fig.29), while the movement of macromolecules is counted in the mobile coordinate system associated with these macromolecules (Lagrange coordinates).
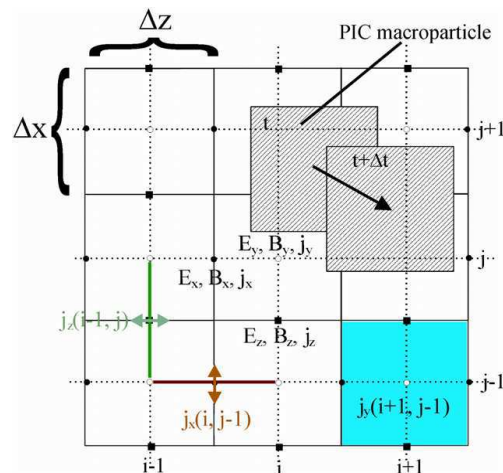

Fig.29 The PIC2D grid structure

The main work cycle of the code has been divided into four parts (Fig.30):
- determination of E and B fields in Euler mesh nodes based on Maxwell equations and using data on concentrations and current densities
- interpolation of E and B fields to the position of macromolecules
- solution of motion equations for macromolecules
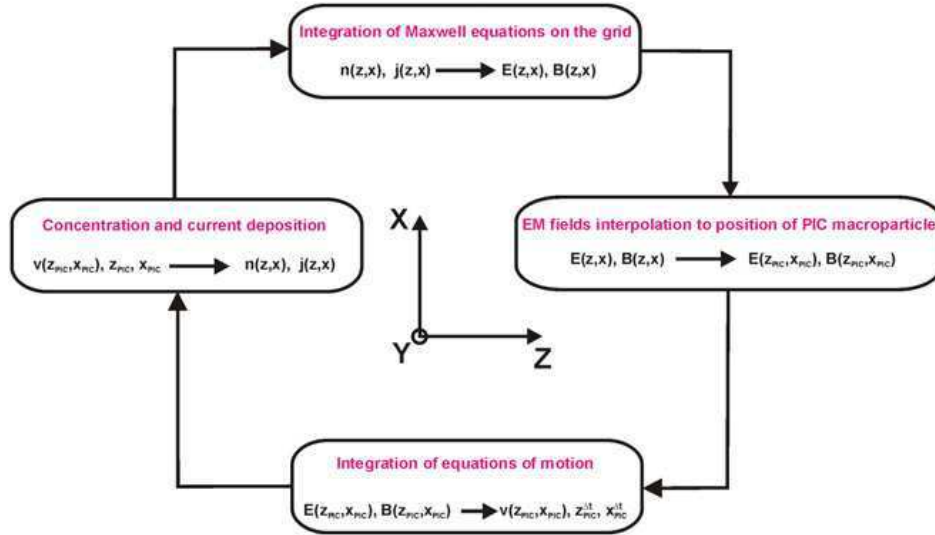- determination of new values of concentration and current density

Fig. 30 The PIC2D code cycle.

Maxwell's equations were solved using the finite difference method and in the first approximation it resembled the scheme developed by Yee. However, unlike the Yee concept, instead of solving the differential equations of the first order, I made transformation of the original Maxwell equations to the form of wave equations (second order), which provided a huge improvement in the stability of the numerical solution. In addition, the code resigns from solving the time-consuming Poisson equation used to determine certain components of electric fields for the precise determination of current density. Current densities were estimated using the Villasenor-Buneman scheme, in which I used recursive procedures, significantly accelerating and simplifying the algorithm used for calculation. In many cases presented in the literature, this scheme was replaced by the 'zig-zag' model developed by Umeda. In order to solve the equations of motion, I used a proven and very precise method of Birsdalel and Langdon, in which the solution of the relativistic equation of motion is divided into three parts: half acceleration with field E, rotation around field B and half acceleration with field E.

As a test, the acceleration of the carbon target with the thickness $L_T = 200$ nm and the preplasma characterized by $L_n = 250$ nm using a laser pulse $\lambda = 800$ nm, $I_L = 2 \times 10^{22}$ W/cm^2 and $\tau_L = 130$ fs (such parameters are available on the ELI laser, generating pulse of energy 1.3 kJ and 10 PW power) was carried out. The calculations were performed for a cavity (LICPA) and no cavity (RPA) case. In the case with a cavity, the target was located 40 μm from the input opening. Data obtained already after a short time (160 fs) of laser beam interaction with the target, showed the advantage of driving ion beams using the LICPA method (maximum ion energies > 1.1 MeV) and simultaneously showed the complex nature of EM fields in the space between the cavity input hole and the driven carbon target (Fig.31).
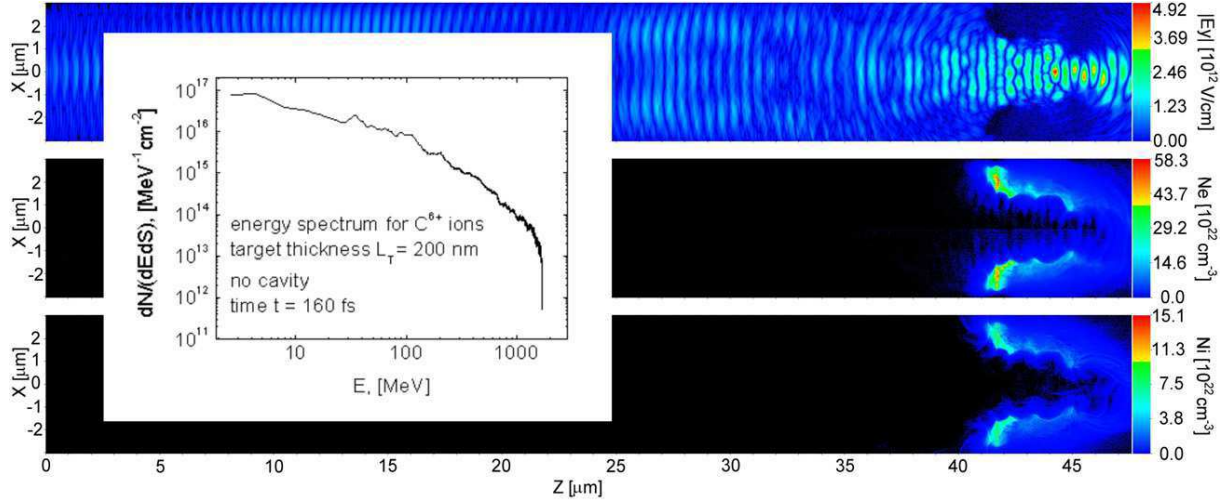
Fig.31 The PIC2D results for laser acceleration of the carbon target for the no cavity scheme at time t = 160 fs. Top—the absolute value of an electric field E_y, middle-concentration of carbon ions, bottom-concentration of electrons, inserted-energy spectrum of the carbon ions. λ = 800 nm, I = 2×10^{22}Wcm^{-2}, τ_L = 130 fs, linear polarization, L_T = 200 nm and L_n = 250 nm.

[A-22] addressed the PIC 1D simulation of investigation of acceleration of ionic carbon targets and heavy (5 µg) micro missiles from gold, using picosecond 100 kJ laser pulses interacting in the LICPA and RPA acceleration regime.

The purpose of experiments with carbon discs was to confirm the possibility of using them as beams initiating the fast ignition process (FI). In the case of gold targets, the aim of the research was to confirm the possibility of producing heavy micro-projectiles.

From the ion beam (protons, carbon ions) to be used as igniters in the inertial confinement process, it is required that their duration is from 5-20 ps, the average ion energy per nucleon is ~ 10-50 MeV amu^{-1}, ion beam intensity $\geq 10^{20}$ W/cm^2, energy fluence should be $\geq$ 2 GJ/cm^2, and the total energy of the beam should be $\geq$ 20 kJ. In addition, it is required that the laser-ion energy transfer coefficient is $\geq$ 15 %. The simulation modeled carbon targets with a thickness of L_T = 8 µm and preplasma with L_n = 0.25 µm, which were placed in a cavity with a reflection coefficient R_c = 0.64 at a distance of L_c = 160 µm from the input hole. For acceleration, an impulse of τ_L = 2 ps, I_L = 2.5 x 10^{21}, 5 x 10^{21}, 8 x 10^{21} W/cm^2 was used. As a result of the simulation, it was found that the beam intensities in the LICPA scheme were 10 times higher than those for the case of RPA, energy fluence was higher 2-4 times depending on the value of I_L. In both cases of acceleration, the relative widths of the energy spectra were similar ($\Delta E_i/\langle E_i \rangle \sim 0.3 - 0.4$), but for LICPA the average ion energies per nucleon were ~ 7.2 to ~ 41 MeV/amu, whereas for RPA it was ~ 2.2 up to ~ 18 MeV/amu. Accordingly, for LICPA η = 23 - 41% and 7 - 18% for RPA. In summary, it was found that for I_L = 5 x 10^{21} W/cm^2 for the LICPA scheme, all parameters of the beam are above the required in the fast ignition process, for RPA these values are twice too small.

In the ignition called "impact ignition" it is required that a heavy projectile weighing 10-6 - 10-4 g is accelerated to speeds above 10^8 cm/s. In the scheme presented by Caruso, these requirements come down to: the mass of the projectile Au ~ 1 µm, the speed 5 x 10^8 cm/s, the minimal kinetic energy 10-20 kJ and the energy fluence ~ 500 MJ/cm^2.

In the calculations the Au^{10+} target with the thickness L_T = 5 µm and preplasma density scale-lenght gradient L_n = 0.25 µm was simulated. Acceleration was made using laser beams with the following parameters: λ = 1.06 µm, τ_L = 10 or 2.5 ps and intensities (for τ_L = 10 ps)

2×10^{20} W/cm^2, 4×10^{20} W/cm^2, 6×10^{20} W/cm^2, (for τ_L = 2.5 ps) 8×10^{20} W/cm^2, 1.6×10^{21} W/cm^2, 2.4×10^{21} W/cm^2. The cavity had a reflection coefficient R_c = 0.75 and the distance between the input hole and the target was equal to L_c = 300 μm. As a result of numerical analysis, it turned out that for the laser energy E_L = 150 kJ corresponding to $I_L = 3 \times 10^{20}$ W/cm^2, (for τ_L = 10 ps) all parameters of the Au projectile meet the ignition conditions required by the "impact ignition" as far as the LICPA scheme of acceleration is concerned, while for the RPA acceleration, the ignition thresholds can only be achieved for lasers with $E_L > 500$ kJ. The relevant parameters achieved for LICPA were as follows: v_p = 7.6 $\times$ 10^8 - 1.6 $\times$ 10^9 cm/s, η = 12 - 21%, F_p = 0.21 - 1.2 GJ/cm^2, for RPA: v_p = 2.4 $\times$ 10^8 - 6.9 $\times$ 10^8 cm/s, η = 1.2 - 3.3%, F_p = 0.01 - 0.2 GJ/cm^2 (Fig.32).
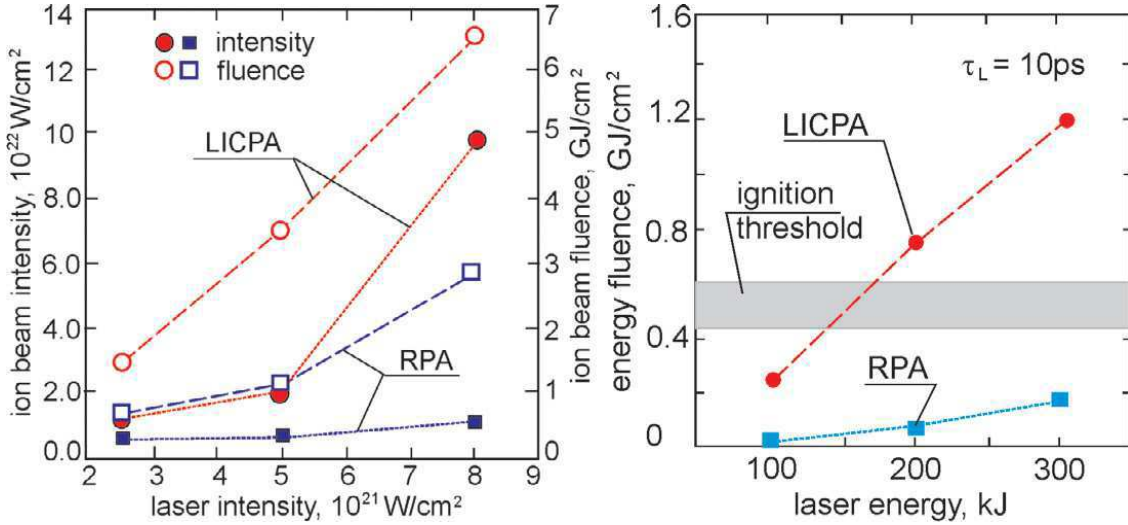

Fig.32 (Left figure) The carbon ion beam intensity and fluence as a function of laser intensity for ion beams produced by LICPA or RPA. (Right figure) The energy fluence of the gold plasma bunch driven by LICPA or RPA as a function of laser energy.

The next step in the research on the acceleration of ion beams based on the LICPA method were numerical studies on the efficiency of producing such beams depending on the parameters of carbon targets and the type of polarization of laser beams. This issue was addressed in paper [A-23]. Using the PIC 1D and PIC 2D modeling, the behavior of carbon targets with thicknesses L_T = 0.2 μm, 0.5 μm, 1.0 μm, 2.0 μm with preplasma density gradient scale-length L_n = 0.25 μm was investigated. In the case of the LICPA method, the target was moved away the input hole to a distance of L_c = 40 μm. In the calculations, it was assumed that the energy of the laser beam with the length λ = 0.8 μm had a constant value regardless of the polarization, which implied that for circular polarization $I_L = 10^{22}$ W/cm^2, and for linear polarization $I_L = 2 \times 10^{22}$ W/cm^2. The pulses were τ_L = 130 fs long. In addition, in the case of 2D modeling, it was assumed that the width of the cavity was 6 μm, and the width of the input hole d = 1.5 μm or 3 μm. The values of beam reflection for 1D simulation determined during the 2D simulation were: for d = 1.5 μm, R_c = 0.64, and for d = 3.0 μm, R_c = 0.51. As a result of 2D calculations, it was noticed that in the case of simulation of LICPA acceleration, due to the formation of a complex structure of electromagnetic fields in the space between the entrance wall and the target, it is possible to create conditions in which different instabilities (such as Rayleigh-Taylor instability) can appear. Such instabilities were the reason of complex ions trajectories, observed during simulation. However, due to the presence of cavity walls, the ions do not diverge, and are additionally exposed to longer acceleration by EM radiation trapped in the cavity, compared to the RPA mechanism. In the case of analyzing the

results from non-cavity acceleration (pure RPA mechanism), the structure of radiation due to the lack of reflections is orderly and straight, however, ions tend to fly out of the effective acceleration area and as a result, the achieved parameters of ion beams are worse than for the LICPA scheme. In spite of the fact that 2D modeling revealed additional physical aspects accompanying the interaction of laser radiation with targets, due to the much faster operation of 1D codes, further investigations were carried out using this type of simulation. In the course of calculations, it was found that the LICPA acceleration leads to a significant improvement in ion beam parameters in relation to RPA acceleration.What proved to be a new finding is that acceleration with circular polarization leads to a significant improvement of the process in comparidon to the case when a linear polarization beam is in use. This phenomenon is explained by the fact that: when using circular polarization, the resultant value of electric and magnetic field vectors has a constant value, and and the only observed change is in the rotation of these vectors in the plane perpendicular to the propagation direction of the EM beam. It leads to generation of smoothed ponderomotive force, responsible for fluent acceleration. In the case of linear polarization, the electric and magnetic field vectors change with the time period equal to T/2 (where T-period of electromagnetic wave oscillation) which in turn leads to the periodic nature of ponderomotive force and deterioration of acceleration conditions. As for the efficiency of laser-target energy transfer, no significant difference between polarizations was noticed, only differences between acceleration schemes. For targets with different thicknesses for LICPA η = 28% - 58%, and for RPA η = 2% - 24% (lower values are achieved for thicker targets, higher for thin targets) (Fig.33).

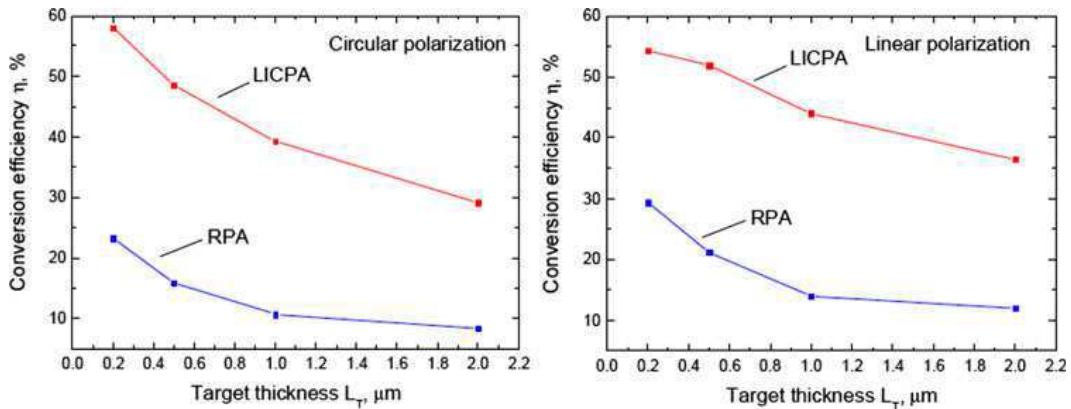Fig.33 Energy conversion efficiency as a function of the target thickness for LICPA and RPA. τ_L =130 fs, I_L = 2 × 10^{22} W/cm^2 (LP), 10^{22} W/cm^2 (CP). Figure made for C^{6+} ions.

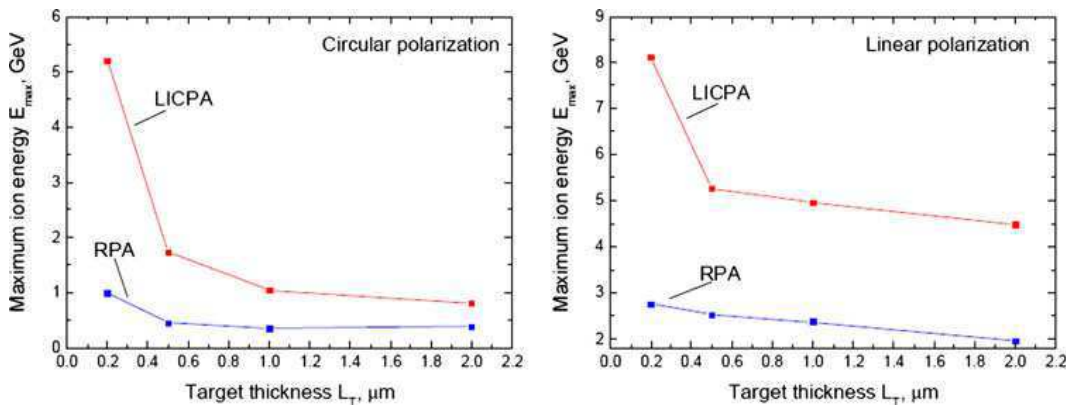The situation changes for the observed maximum energy of C^{6+} ions (Fig.34).

Fig.34 Maximum ion energy as a function of the target thickness for LICPA and RPA. τ_L = 130 fs, I_L = 2 × 10^{22} W/cm^2 (LP), 10^{22} W/cm^2 (CP). Figure made for C^{6+} ions.

For linear polarization, the dominant effect is TNSA acceleration (target normal sheath acceleration) leading to the formation of higher energy ions, but in relatively small amounts compared to RPA acceleration. The second of the above-mentioned mechanisms is supported by the circular polarization of the EM wave, leading to the formation of ion beams with lower energies, but with much higher densities. Generally and intuitively, a decrease in basic beam parameters was observed (average energy, laser-plasma energy transfer efficiency and maximum ion energy) with the increase of the target thickness.

The publication [A-24] summarizes several years of our research on acceleration issues using the LICPA method and its comparison with acceleration made without the use of a cavity. The paper presents the results of experimental tests carried out on the PALS laser system in Prague. In the experiment carried out in the hydrodynamic regime ($I_L \leq 10^{17}$ W/cm^2 i $\tau_L > 10$ ps), where the dominant effect responsible for acceleration is the pressure of hot plasma in the cavity area, a huge improvement in all parameters of plasma missiles was demonstrated when the cavity was used (LICPA method) compared to the no-cavity method (Fig.35).
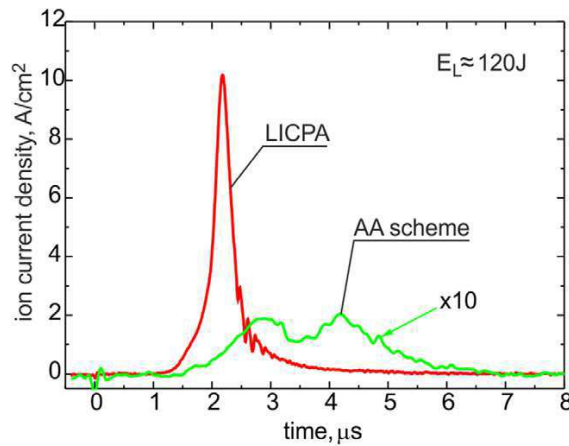

Fig.35 The TOF ion signals for the ion beam driven by LICPA or AA recorded on the laser beam axis at the distance of 30 cm from the irradiated CD$_2$ target.

In all cases aluminum targets with the following thicknesses: 10 μm, 20 μm, 50 μm, 75 μm coated with a polyethylene ablator, 5 μm thick, accelerated by a laser beam with a length of $\tau_L = 0.3$ ns, $I_L \sim 10^{15}$ W/cm^2 and placed in the cavity at a distance of $L_c = 400$ μm from the input hole, the occurrence of dense aluminum missiles at speeds of up to ~ 100 km/s was observed at the outlet of the cavity. In the case of acceleration without a cavity in the starting area, only the appearance of low density CH plasma was observed, while the aluminum part of the target was only slightly accelerated.

The second component of the work was the presentation of the simulation results for the LICPA method and the no-cavity drive, carried out for the radiation photon acceleration (RPA) regime. In these calculations, acceleration using short laser pulses of high intensity ($\tau_L << 1$ ps, $I_L \geq 10^{19}$ W/cm^2) was investigated (Fig.36).
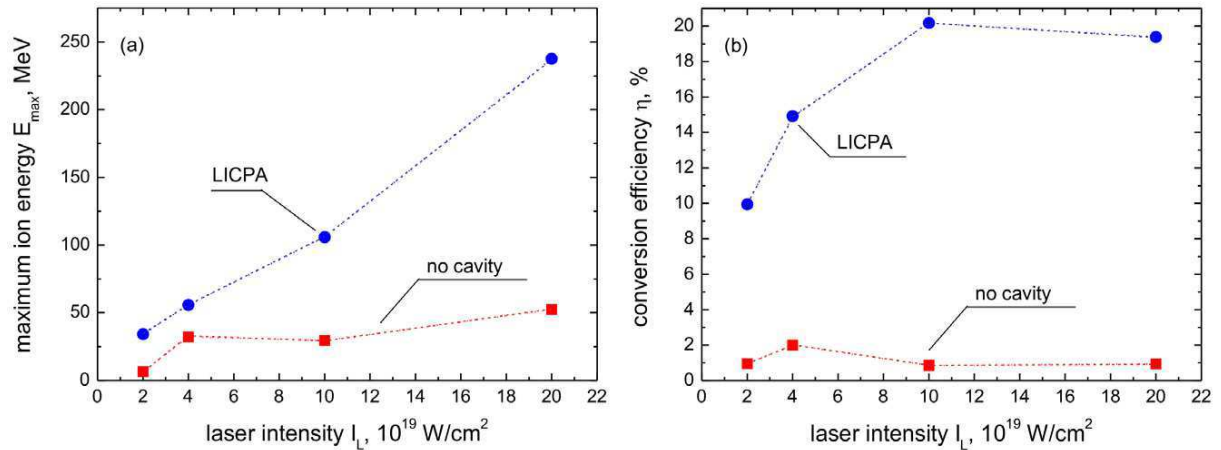
Fig.36 The maximum ion energy (*a*) and the laser-ions energy conversion efficiency (*b*) for ion beams driven in the LICPA accelerator or the conventional scheme (no cavity) as a function of laser intensity on the carbon target. The result of 1D PIC simulations for $L_T = 50$ nm, $L_c = 100$ μm and the linear light polarization.

It has been shown that both in the case of driving carbon targets and bullets from materials with a large Z (eg Au), the advantage of using the LICPA method over the no-cavity method is undeniable. In the case of lightweight carbon targets, it is possible to obtain parameters sufficient to implement fast ignition (FI), i.e. ion beams of 5 - 10 ps length with an average energy of 10-50 MeV/amu, intensities $\geq 10^{20}$ W/cm^2, energy fluence ≥ 2 GJ/cm^2 and total energy ≥ 20 kJ with laser-plasma energy transfer efficiency > 15%. In the case of acceleration of heavy projectiles for the purpose of kinetic ignition using the LICPA method, as previously, parameters sufficient to achieve this goal are obtained. Such powered missiles with masses of ~ 1 μg obtain speeds of ~ 5 x 10^8 cm/s.

In the years 2014-2018 I dealt with the following issues:
- I participated in the design works on the X-ray spectrometer, working in the quantum counting regime (Pulse Height Analyzer) and in the work on tools for processing and analyzing data obtained as a result of the operation of this device.
- I participated in the work on GEM detectors applicable in the diagnosis of soft X-rays (creation of a program simulating energy spectra registered by GEM detectors)

From 2014 to the present I have been involved in the works on the design of diagnostics for the needs of plasma research inside toroidal devices with strong magnetic fields as well as the processing of results obtained as a result of the use of these devices. Based on the MAST code, created by me in 2008, designed to simulate X-ray radiation from a plasma produced in a British MAST device, I created a RayX computer code simulating X-ray emission from a low density plasmas from tokamaks or stellarators, taking into account the real geometry of plasma devices and plasma itself. The program includes three basic components of X-rays: free-free, free-bound, bound-bound radiation from the main component of the plasma and from impurities (eg Fe, C, O, etc.).
As part of the simulation, different types of plasma radiation could be modeled on the basis of the predicted or measured shapes of temperature profiles and electron concentration with the assumption of coronal ionization equilibrium. As part of the detector modeling, it was possible to obtain information on the number of registered photons in the function of their

energy, for arbitrarily set slits widths, their distance from the detector and the location of the entire device relative to the plasma. The description of the program can be found in the paper [B07]. Fig.37 presents a sample user interface view used for setting diagnostic simulation parameters.
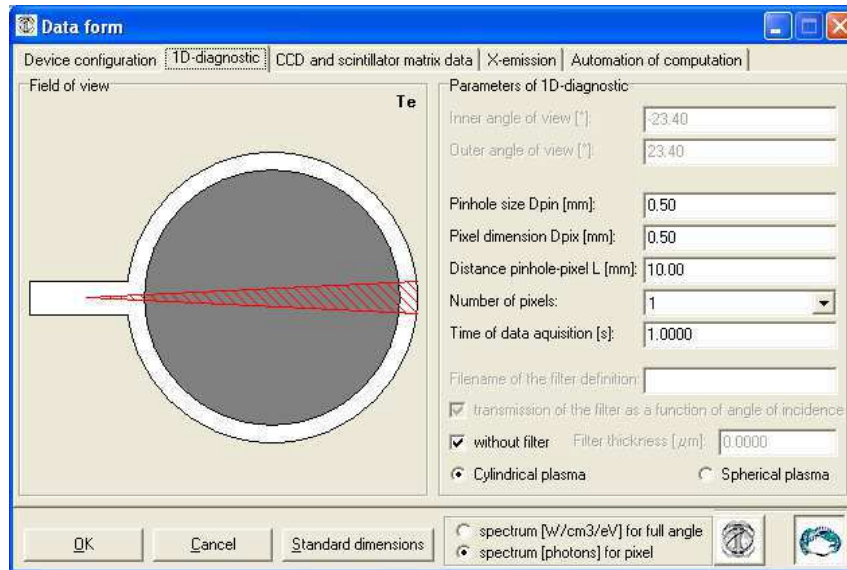

Fig.37 RayX user interface (setting of the diagnostic parameters)

In the given literature item, one can find some sample results of PHA device simulations (Pulse Height Analyzer), made by our team for the world's largest Wendelstein W7-X stellarator in Greifswald. These examples were a supplement to the program description. The results of the computational and design work led to the successful completion of the PHA system and testing it, as part of experimental campaigns in 2016 (OP1.1) and 2017 (OP1.2a).

What is more, I am the author of the software called PHAControlPanel, which controls the above-mentioned diagnostic. This program enables starting and controlling all basic PHA device modules, i.e. high and low voltage power supply of detectors, XIA Mercury spectrophotometer voltage, piezo slit system voltage and filter selection. to the program enables us to set the parameters of the spectrometer (peaking time, gap time, etc.), calibrate the detectors using an X-ray tube and examine the correlation between the voltages generated by the DT modules that manage the gap widths and beryllium filter positions. The program also enabled the start and completion of the process of acquisition of X-rays quanta (manual starting and stopping or triggered automatically by W7-X stellarator trigger signals) and sending the registered data to the central database. The look of the main user interface is presented in Fig.38.
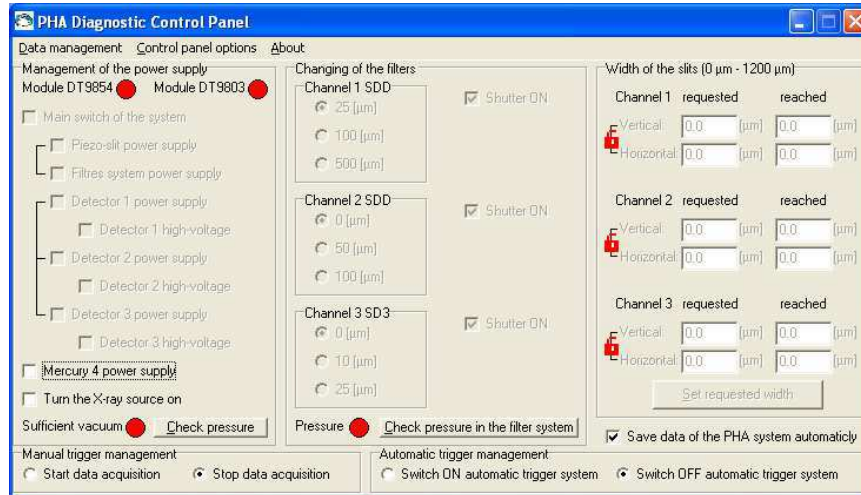
Fig.38 PHAControlPanel user interface for controlling PHA diagnostic.

In 2016 and 2017, I created a universal dynamic library XRayLib.dll, containing a set of functions and procedures that enable convenient simulation of X-rays for various ionic compositions of impurities in plasma. On the basis of this library, I wrote a series of codes for the analysis of data obtained as a results of measurement made by the use of PHA diagnostic. Among them, the Zefirex program for a comprehensive analysis of registered X-ray spectra. The program was able to take into account the real geometry of the measurement system and plasma (gaps sizes, detector distance from gaps, distance and plasma shape) allowing for the conversion of original results expressed as the number of photons per keV into the average plasma emissivity $\varepsilon[W/eV/m^3]$ in the area of the detector's cones of view. With such a transformed spectrum, it was possible to perform computer simulations taking into account the observed impurities and determine the Z_{eff} values using the data on electron concentration n_e and the electron temperature T_e, obtained from the Thomson Scattering diagnostics (Fig. 39).

Another program based on the XrayLib.dll library was the Linex code to identify emission lines of impurities for 22 elements. Fig.40 presents the user interface.
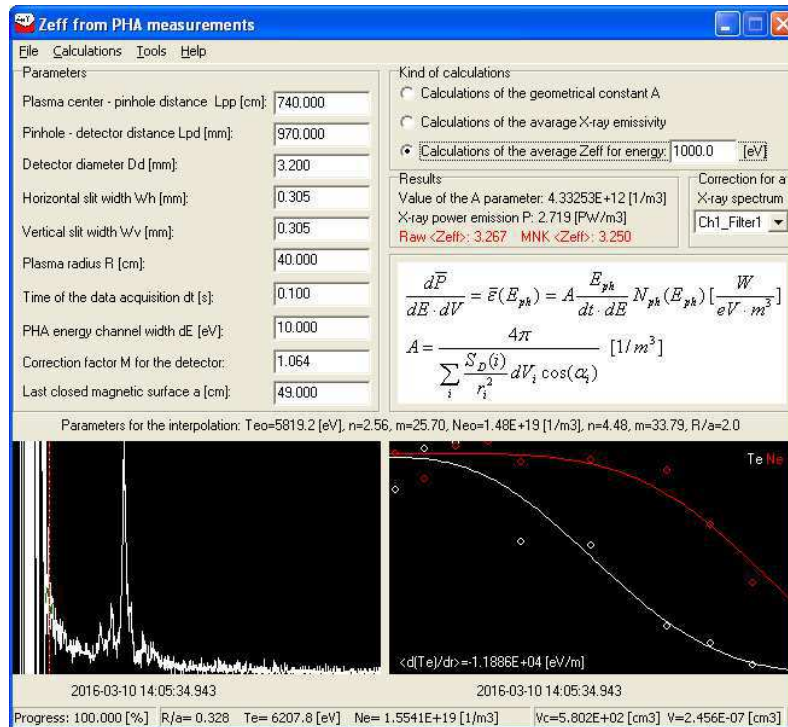
Fig.39 The user interface of the Zefirex program (spectrum registered during the OP1.1 campaign).
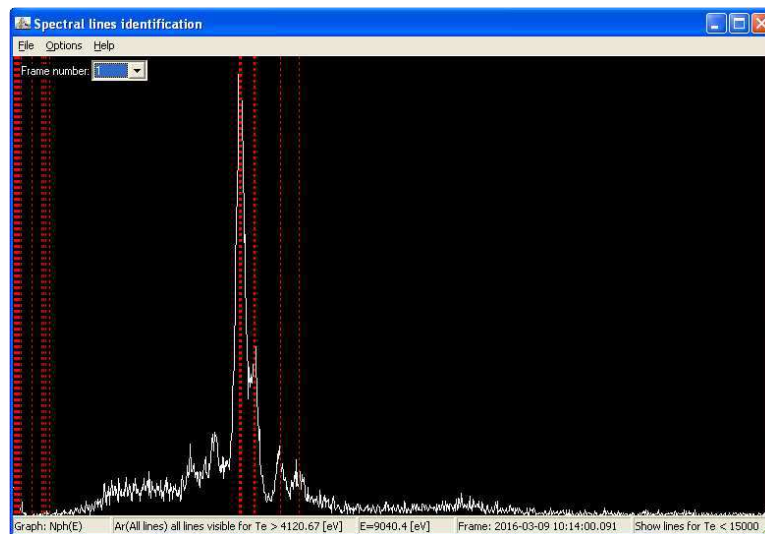

Fig.40 Linex user interface (identification of the Ar line for the raw spectrum obtained during the OP1.1 campaign).

The results of works related to the acquisition and interpretation of data registered by the PHA system and the work related to the next detection system called MFS (Multi-Foil Sytem) in which I had my share, can be found in the works [B-08, B-09, B-10 , B-11, B-12].

As part of the GEM project, I was responsible for creating a computer code that allows simulation of energy spectra that can be recorded by single and two-dimensional GEM matrices, working in the X-ray range, including real (3D) geometry of the detector system and real concentration distributions and electron temperature on tokamaks, and especially for the WEST device. The program was made on the basis of the XRayLib.dll library and modeled the emission of X-rays based on the corona balance in plasma and taking into account emissions such as free-free, free-bound and bound-bound. The user interface is shown in

Fig.41. The description of the whole project of which I was a co-author, including the scope of GEM detector applications, can be found in [B-13, B-14, B-15].
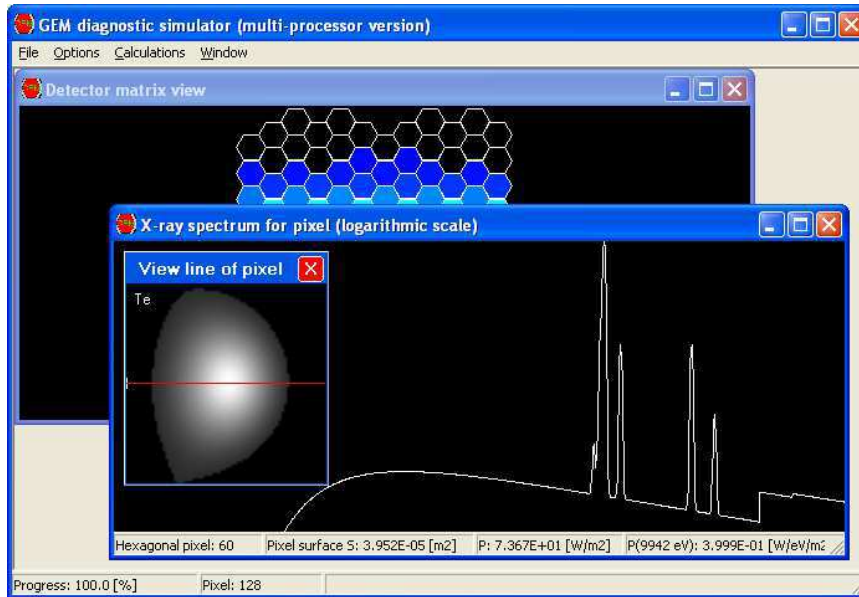

Fig.41 The user interface of the GEM-MP program with sample calculation results for real T_e and n_e profiles from WEST tokamak, for the GEM-2D matrix.

References

I. List of publications constituting the scientific achievement referred to in art. 16 sec. 2 of the Act

[A-01] J. Badziak, S. Głowacz, **S. Jabłoński**, P. Parys, J. Wołowski and H. Hora, *"Production of ultrahigh-current-density ion beams by short-pulse skin-layer laser–plasma interaction"*, Applied Physics Letters 85, 3041 (2004)

[A-02] J. Badziak, S. Głowacz, **S. Jabłoński**, P. Parys, J. Wołowski, H. Hora, J. Krása, L. Láska and K. Rohlena, *"Production of ultrahigh ion current densities at skin-layer subrelativistic laser–plasma interaction"*, Plasma Physics and Controlled Fusion 46 (2004) B541–B555

[A-03] S.Głowacz, J. Badziak, **S. Jabłonski**, H. Hora, *"Numerical modelling of production of ultrahigh-current-density ion beams by short-pulse laser-plasma interaction"*, Czechoslovak Journal of Physics (2004) 54 (Suppl 3)

[A-04] J. Badziak, S. Głowacz, **S. Jabłoński**, P. Parys, J. Wołowski and H. Hora, *"Generation of picosecond high-density ion fluxes by skin-layer laser-plasma interaction"*, Laser and Particle Beams (2005), 23, 143–147

[A-05] J. Badziak, S. Głowacz, **S. Jabłoński**, P. Parys, J. Wołowski, and H. Hora, *"Laser-driven generation of high-current ion beams using skin-layer ponderomotive acceleration"*, Laser and Particle Beams (2005), 23, 401– 409

[A-06] **S. Jabłoński**, H. Hora, S. Głowacz, J. Badziak, Yu Cang and F. Osman, *"Two-fluid computations of plasma block dynamics for numerical analyze of rippling effect"*, Laser and Particle Beams (2005), 23, 433– 440

[A-07] J. Badziak, **S. Jabłoński**, S. Głowacz, *"Generation of highly collimated high-current ion beams by skin-layer laser-plasma interaction at relativistic laser intensities"*, Applied Physics Letters 89, 061504 (2006)

[A-08] S. Glowacz, H. Hora, J. Badziak, **S. Jablonski**, Yu Cang, and F. Osman, *"Analytical description of rippling effect and ion acceleration in plasma produced by a short laser pulse"*, Laser and Particle Beams (2006), 24, 15–25

[A-09] J. Badziak, S. Głowacz, H. Hora, **S. Jabłoński**, and J. Wołowski, *"Studies on laser-driven generation of fast high-density plasma blocks for fast ignition"*, Laser and Particle Beams (2006), 24, 249– 254

[A-10] **S. Jabłoński**, J. Badziak, S. Głowacz, *"2D hydrodynamic simulations of generation of high current proton beams by relativistic skin-layer laser-plasma interaction"*, Czechoslovak Journal of Physics 56, (2006), B485-B492, Suppl. B

[A-11] J. Badziak and **S. Jabłoński**, *"Focusing of high-current laser-driven ion beams"*, Applied Physics Letters 99, 151503 (2007)

[A-12] H. Hora, J. Badziak, M. N. Read1, Yu-Tong Li, Tian-Jiao Liang, Yu Cang, Hong Liu, Zheng-Ming Sheng, Jie Zhang, F. Osman, G. H. Miley, Weiyan Zhang, Xiantu He, Hansheng Peng, S. Glowacz, **S. Jablonski**, J. Wolowski, Z. Skladanowski, K. Jungwirth, K. Rohlena, and J. Ullschmied, *"Fast ignition by laser driven particle beams of very high intensity"*, Physics of Plasmas 14, 072701 (2007)

[A-13] J.Badziak and **S. Jabłoński**,and J Wołowski, *"Progress and prospect of fast ignition of ICF targets"*, Plasma Physics and Controlled Fusion 49, (2007) B651–B666

[A-14] J.Badziak, **S. Jabłoński**, P. Parys, M. Rosiński, J. Wołowski, A. Szydłowski, P.Antici, J. Fuchs, and A. Mancic, *"Ultraintense proton beams from laser-induced skin-layer ponderomotive acceleration"*, Journal of Applied Physics 104, 063310 (2008)

[A-15] J.Badziak, **S. Jabłoński**, P. Parys, M. Rosiński, J. Wołowski, A. Szydłowski, P.Antici, J. Fuchs, A. Mancic, *"Generation of Ultraintense Proton Beams Driven by a Short-Pulse Multi-TW Laser"*, Photonics Letters of Poland, vol.1 (1), 22-24 (2009)

[A-16] J. Badziak and **S. Jabłoński**, *"Ultraintense ion beams driven by a short-wavelength short-pulse laser"*, Physics of Plasmas 17, 073106 (2010)

[A-17] J. Badziak, **S. Jabłoński**, P. Parys, A. Szydłowski, J. Fuchs and A. Mancic, *"Production of high-intensity proton fluxes by a 2ωNd:glass laser beam"*, Laser and Particle Beams (2010), 28, 575–583

[A-18] J. Badziak and **S. Jabłoński**, *"Acceleration of a solid-density plasma projectile to ultrahigh velocities by a short-pulse ultraviolet laser"*, Applied Physics Letters 99, 071502 (2011)

[A-19] J. Badziak, **S. Jabłoński**, T. Pisarczyk, P. Rączka, E. Krousky, R. Liska, M. Kucharik, T. Chodukowski, Z. Kalinowska, P. Parys, M. Rosiński, S. Borodziuk, and J. Ullschmied, *"Highly efficient accelerator of dense matter using laser-induced cavity pressure acceleration"*, Physics of Plasmas 19, 053105 (2012)

[A-20] J. Badziak, **S. Jabłoński**, and P. Rączka, *"Highly efficient generation of ultraintense high- energy ion beams using laser-induced cavity pressure acceleration"*, Applied Physics Letters 101, 084102 (2012)

[A-21] **S. Jabłoński**, *"Two-dimensional relativistic particle-in-cell code for simulation of laser- driven ion acceleration in various acceleration schemes"*,
Physica Scripta T161 (2014) 014022

[A-22] J. Badziak, **S. Jabłoński**, *"Efficient acceleration of dense plasma bunches for fusion-related applications in the LICPA accelerator"*,
Physica Scripta (2014) T161, :014031

[A-23] **S. Jabłoński**, J.Badziak, P. Rączka, *"Generation of high-energy ion bunches via laser-induced cavity pressure acceleration at ultra-high laser intensities"*,
Laser and Particle Beams (2014) 32, :129-135

[A-24] J. Badziak, M. Rosiński, **S. Jabłoński**, T. Pisarczyk, T. Chodukowski, P. Parys, P. Rączka, E. Krousky, J. Ullschmied, R. Liska and M. Kucharik,
"Enhanced efficiency of plasma acceleration in the laser-induced cavity pressure acceleration scheme",
Plasma Physics and Controlled Fusion 57 (2015) 014007

II. List of published (not included in the achievement mentioned in point. I) scientific papers

[B-01] J. Badziak and **S. Jablonski**, *"Generation of picosecond pulses by fast periodic Q-switching in KrF excimer laser with saturable absorber"*,
Optics Communications 103 (1993), 277-284

[B-02] J. Badziak and **S. Jablonski**, *"Nonlinear uv pulse compression in a multipass KrF excimer amplifier with a saturable absorber"*,
Optics Communications 112 (1994), 181-188

[B-03] J. Badziak and **S. Jablonski**, *"Ultrashort-pulse generation in excimer lasers by fast mode locking using electrooptic deflector"*,
IEEE Journal of Quantum Electronics 33 (1997), 490-499

[B-04] J. Badziak and **S. Jablonski**, *"Generation of ultrashort pulses in short-gain-duration lasers by fast mode-locking"*,
Proc. SPIE 3186, Laser Technology V: Physics and Research and Development Trends, 72 (1997)

[B-05] J. Badziak and **S. Jablonski**, *"Modelling of short-pulse generation in rare-gas halide excimer lasers. Part I. The model and its verification"*,
Journal of Modern Optics 46 (1999), 509-528

[B-06] J. Badziak and **S. Jablonski**, *"Modelling of short-pulse generation in rare-gas halide excimer lasers. Part II. Numerical investigation of KrF and XeCl lasers with a square-wave-driven pockels modulator"*,
Journal of Modern Optics 46 (1999), 773-785

[B-07] **S. Jabłoński**, A. Czarnecka, M. Kubkowska, L. Ryć, A. Weller, C. Biedermann, R. Konig and the W7-X Team, *"Simulation of pulse height analysis soft X-ray

spectra expected from W7-X",
Journal of Instrumentation 10 (2015), P10021

[B-08] M. Kubkowska, A. Czarnecka, W. Figacz, **S. Jabłoński**, J. Kaczmarczyk,
N. Krawczyk, L. Ryć, C. Biedermann, R. Koenig, H. Thomsen, A. Weller
and W7-X team, „*Laboratory tests of the Pulse Height Analysis system
for Wendelstein 7-X"*,
Journal of Instrumentation 10 (2015) P10016

[B-09] T. Sunn Pedersen, M. Otte, S. Lazerson, P. Helander, S. Bozhenkov, C. Biedermann,
T. Klinger, R.C. Wolf, H.-S. Bosch & The Wendelstein 7-X Team (.., **S. Jablonski**,..),
*"Confirmation of the topology of the Wendelstein 7-X magnetic field to better than
1:100,000"*,
Nature Communication, (2016) DOI: 10.1038/ncomms13493

[B-10] N. Krawczyk, C. Biedermann, A. Czarnecka, T. Fornal, **S. Jablonski**, J. Kaczmarczyk,
M. Kubkowska, F. Kunkel, K. J. McCarthy, L. Ryc, H. Thomsen, A. Weller, W7-X
team, *"Commissioning and first operation of the pulse-height analysis diagnostic on
Wendelstein 7-X stellarator"*,
Fusion Engineering and Design 123 (2017) 1006–1010

[B-11] M. Kubkowska, T. Fornal, J. Kaczmarczyk, **S. Jabłonski**, W. Figacz, L. Ryć,
H. Thomsen, U. Neuner, A. Weller, the W7-X team, *"Conceptual design of the
multi-foil system for the stellarator W7-X"*,
Fusion Engineering and Design 123 (2017) 811–815

[B-12] M. Kubkowska, A. Czarnecka, T. Fornal, M. Gruca, N. Krawczyk,
S. Jabłoński, L. Ryć, H. Thomsen, K. J. McCarthy, C. Biedermann, B. Buttenschön,
A. Alonso, R. Burhenn, W7-X team, *"First Results from the Soft X-ray Pulse Height
Analysis System on Wendelstein 7-X Stellarator"*,
Fusion Engineering and Design, in press

[B-13] M. Chernyshova, T. Czarski, **S. Jabłoński**, E. Kowalska-Strzęciwilk, K. Poźniak;
G. Kasprowicz; W. Zabołotny; A. Wojeński; A. Byszuk; M. Burza; B. Juszczyk;
P. Zienkiewicz, „*Development of 2D imaging of SXR plasma radiation by means of
GEM detectors"*,
Photonics Applications in Astronomy, Communications, Industry, and High-
Energy Physics Experiments 2014

[B-14] D. Mazona, M. Chernyshova, G. Jiolat, T. Czarski, P. Malard, E. Kowalska-
Strzeciwilk, **S. Jablonski**, W. Figacz, R. Zagorski, M. Kubkowska, G. Kasprowicz,
K. Pozniak,W. Zabolotny, S. Larroque, J.-M. Verger, M. O'Mullane, J. Mlynar,
A. Byszuk, A. Wojenski, *"Design of soft-X-ray tomographic system in WEST
using GEM detectors"*,
Fusion Engineering and Design 96–97 (2015) 856–860

[B-15] A.J. Wojenski, G. Kasprowicz, K.T. Pozniak, A. Byszuk, M. Chernyshova, T. Czarski,
S. Jablonski, B.Juszczyk, P.Zienkiewicz, „*Multichannel reconfigurable measurement
system for hot plasma diagnostics based on GEM-2D detector"*,
Nuclear Instruments and Methods in Physics Research B 364 (2015) 49–53

Summary contains 40 numbered pages.

July 5, 2018

S. Jabłoński